The Influence of the Magmatic to Postmagmatic Evolution of the Parent Rock on the Co Deportment in Lateritic Systems: The Example of the Santa Fé Ni-Co Deposit (Brazil)

F. Putzolu,[1] L. Santoro,[2,3,†] C. Porto,[4] N. Mondillo,[1,2] M. Machado,[4] B. Saar De Almeida,[1] A. Bastos,[5,6] and R. Herrington[2]

[1]*Dipartimento di Scienze della Terra, dell'Ambiente e delle Risorse, Università di Napoli "Federico II" Complesso Universitario di Monte S. Angelo, Via Cintia 26, Napoli 80126, Italy*

[2]*Earth Sciences Department, Natural History Museum, Cromwell Road, London SW7 5BD, United Kingdom*

[3]*Università degli studi di Torino, Dipartimento di Scienze della Terra, Via Valperga Caluso 35, Torino 10125, Italy*

[4]*Instituto de Geociências da Universidade Federal do Rio de Janeiro, Av. Athos da Silveira Ramos, 274-Cidade Universitária-Ilha do Fundão, Rio de Janeiro, Brazil*

[5]*Programa de Pós-Graduação em Avaliação de Impactos Ambientais (PPGAIA) Universidade La Salle, Victor Barreto 2288, Canoas, Rio Grande do Sul, Brazil*

[6]*Programa de Pós Graduação em Geociências (PPGGEO), Universidade Federal do Rio Grande do Sul, Av. Bento Gonçalves 9500, Porto Alegre, Rio Grande do Sul, Brazil*

Abstract

The Santa Fé Ni-Co deposit is a major undeveloped lateritic deposit located in the Goiás State of Central Brazil. The deposit comprises two properties that together have indicated resources of 35.7 million tonnes (Mt), grading 1.14% Ni and 0.083% Co, and inferred resources of 104.3 Mt at 1.03% Ni and 0.054% Co. The laterite was derived from Late Cretaceous alkaline ultramafic lithologies that experienced an initial silicification from Eocene to Oligocene, followed by lateritization and partial reworking in Miocene-Pliocene. The deposit is characterized both by oxide- and phyllosilicate-dominated ore zones. In the former, Ni- and Co-bearing hematite and goethite dominate the supergene mineralogical assemblage, while ore-bearing Mn oxyhydroxides occur as minor components. In the phyllosilicate-dominated horizons the major Ni-carrying phase is chlorite.

Multivariate statistical analyses (factor analysis and principal components analysis) conducted on the drill core assay database (bulk-rock chemical analyses) showed that significant differences exist between Ni and Co distributions. The Ni distribution is not controlled by any clear geochemical correlation. This is because the highest Ni concentrations have been measured in the ferruginous and in the ochre saprolite zones, where Ni-bearing minerals (chlorite and goethite) are mostly associated with reworked material and only in a limited way, with zones affected by in situ ferrugination. Cobalt has an atypical statistical distribution at Santa Fé if compared with other laterites, correlated not only with Mn but also with Cr in the majority of the laterite facies. From microchemical analyses on several potential Co-bearing minerals, it was found that the Co-Cr association is related to elevated Co contents in residual spinels, representing unweathered phases of the original parent rock now included in the laterite. This element distribution is atypical for Ni-Co laterite deposits, where Co is normally associated with Mn in supergene oxyhydroxides. In the case of the Santa Fé laterite, the Co concentration in spinels is likely related to magmatic and postmagmatic processes that affected the original parent rock before lateritization, specifically (1) orthomagmatic enrichment of Co in chromite, due to its high affinity to spinels in alkaline melts, and (2) trace elements (i.e., Co, Mn, Ni, and Zn) redistribution during the hydrothermal alteration of chromite into ferritchromite. The Santa Fé deposit represents a good example of how the prelateritic evolution of a parent rock strongly affects the efficiency of Co mobilization and enrichment during supergene alteration. Based on the interpretation of metallurgical test work, a fraction of total Co between 20 and 50% is locked in spinels.

Introduction

Nickel laterite deposits are the product of weathering of ultramafic parent rocks at tropical latitudes (Gleeson et al., 2003; Freyssinet et al., 2005; Butt and Cluzel, 2013; Herrington et al., 2016). During lateritization, interaction between ferromagnesian minerals in the subaerial environment and acid soil solutions enhances leaching of mobile cations (e.g., Si, Mg) from primary minerals and residual enrichment of transition metals in newly formed phases, such as oxyhydroxides and phyllosilicates (e.g., Golightly, 2010). Nickel laterites often

contain economically exploitable reserves of Ni and Co (e.g., Freyssinet et al., 2005; Mudd and Jowitt, 2014), accounting for about 60% of worldwide Ni resources. Brazilian Ni reserves consist of 11,000,000 t, which represent approximately 12% of the total global reserves (U.S. Geological Survey, 2020).

The general features of a laterite profile, such as the mineralogy and chemistry, are products of the interplay between many factors, such as climate, relief, drainage conditions, tectonic lineaments, parent rock mineralogy, and degree of serpentinization (Gleeson et al., 2003; Freyssinet et al., 2005; Golightly, 2010; Porto, 2016; Putzolu et al., 2019). Nickel laterites can be subdivided in three main types: (1) oxide-type deposits, charac-

† Corresponding author: e-mail, licia.santoro85@gmail.com

837

terized by laterite profiles dominated by a ferruginous saprolite (i.e., ferruginous saprolite horizon or oxide zone), where Ni is hosted in Fe and Mn oxyhydroxides, (2) clay-type deposits, dominated by Ni-bearing smectites occurring in massive and poorly jointed saprolite units, and (3) hydrous Mg silicate deposits, also called "garnierite-type," where Ni is hosted in mineralogically complex mixtures of serpentine, talc, and sepiolite occurring as vein filling and cement in faults and open spaces in the saprolite unit (Butt and Cluzel, 2013, and references therein). The genetic dynamics between these deposit types are significantly different, as oxide-type and smectite-type ores develop from a continuous lateritization process in stable terranes, whereas in garnierite-type ores, lateritization depends on the lowering of the water table and, thus, on the leaching level within the weathering profile. Moreover, the formation of cracks and open spaces is crucial for garnierite precipitation (Cluzel and Vigier, 2008; Butt and Cluzel, 2013, and references therein; Villanova-de-Benavent et al., 2014). Several studies have highlighted the fact that the original features of the magmatic bedrock can exert a primary role in defining the Ni mineralogy and fertility in laterite ores. For example, the alteration of olivine-rich cumulates (i.e., dunite) generally produces oxyhydroxide-dominated ores, whereas the alteration of pyroxene-rich bedrocks (i.e., peridotite and pyroxenite) gives rise to laterites containing well-developed Ni-rich clay zones (e.g., Freyssinet et al., 2005, and references therein). Furthermore, Lambiv Dzemua and Gleeson (2012) showed that the variable mineralogy of the Ni carriers in the ultramafic parental rocks, and in particular the differential weathering rate of Ni-bearing phases, can play a primary role in defining the Ni fertility of laterites deposits. Another significant aspect to consider is that many laterite ores can experience postformation diagenetic-metadiagenetic stages that can enhance the ore redistribution. For example, in some Greek laterites, it was shown that Co and other transition metals (i.e., Mn and Zn) can be concentrated in chromite grains, due to the onset of a more reducing environment after the main supergene event (Economou-Eliopoulos, 2003).

The Santa Fé Ni-Co laterite deposit (property of Companhia Niquel Santa Fé Ltda., held 75% by Mineradora INVI Ltda.) is one of the largest unexploited deposits of the South Goiás alkaline province (Brod et al., 2005), with an indicated resource of 35.7 million tonnes (Mt), grading 1.14% Ni and 0.083% Co, and inferred resources of 104.3 Mt, grading 1.03% Ni and 0.054% Co (Dreisinger et al., 2008). Although the ore potential of the Santa Fé deposit is relatively high, the specific mineralogical and geochemical features of the deposit are still poorly known. The aim of this work is to shed new light on the genesis, the nature of the main ore-carrier phases, and the Ni and Co deportment within the deposit. A particular focus will be on how the original geochemistry and nature of the magmatic parent rock and its alteration history acted on the Co deportment during supergene alteration and thus on the metal recovery.

Regional Geology

The Santa Fé Ni-Co laterite deposit originated from the weathering of the Santa Fé ultramafic massif (Fig. 1A, B). Mafic to ultramafic complexes crop out throughout the Brazilian Shield and represent common exploration targets for both hypogene and supergene Ni ores. The Goiás State in Central Brazil is

home to Ni resources associated with two types of ultramafic complexes, which differ in emplacement ages and petrological characteristics (de Oliveira et al., 1992, and references therein). The oldest ultramafic massif is the Tonian Goiás Stratiform Complex, which is part of the Goiás Massif. The Tonian Goiás Stratiform Complex is located in the northeastern sector of the Goiás State and is considered one of the biggest mafic to ultramafic complexes worldwide. The emplacement of the Tonian Goiás Stratiform Complex is believed to be Mesoproterozoic to Neoproterozoic in age (800–770 Ma; Pimentel et al., 2000; Giovanardi et al., 2017), although its geodynamic setting is still a matter of debate. Many authors (e.g., Pimentel et al., 2004, 2006; Giovanardi et al., 2017) suggested that continental rift and back-arc extension in continental crust settings are the most appropriate geodynamic scenarios for the Tonian Goiás Stratiform Complex emplacement. The Tonian Goiás magmatic sequence consists of layered mafic to ultramafic units, such as norites, gabbros, peridotites, pyroxenites, and anorthosites. The mafic basal zone hosts elevated Cu and Ni sulfide concentrations, whereas chromite pods occur in the ultramafic zone of the complex (de Oliveira et al., 1992). Lateritic weathering of the Proterozoic massifs has produced the world-class Niquelândia and Barro Alto Ni deposits (Colin et al., 1990; de Oliveira et al., 1992).

The youngest ultramafic massif is the Late Cretaceous (86.7 Ma) South Goiás alkaline province (Sonoki and Garda, 1988; de Oliveira et al., 1992), which hosts the Santa Fé deposit. The Goiás alkaline province lithologies are located in the southwestern sector of the Goiás State, surrounded by the Paleozoic to Cretaceous Paraná basin (Fig. 1A). The alkaline ultramafic massif consists of scattered and relatively small plutons, which intruded into the Precambrian basement of the Brazilian belt (Valeriano et al., 2008). Almeida (1967, 1983) proposed that the Goiás alkaline province formed during multiple alkaline magmatic events related to the opening of the southern Atlantic Ocean. In contrast, other authors (Gibson et al., 1995; Van Decar et al., 1995) suggested that alkaline magmatism in the Goiàs region could have been due to a mantle plume impacting the Brazilian basement. The Goiás alkaline province is characterized by significant spatial changes in the dominant magmatic and volcanic lithologies: the plutonic alkaline mafic to ultramafic complexes are mainly located in the northern zone, whereas the subvolcanic bodies and their volcanic products are dominant in the central and southern zones, respectively (Brod et al., 2005, and references therein). The subvolcanic bodies are mainly kamafugites, whereas the volcanic products consist of a kamafugite-carbonatite association. The Santa Fé alkaline ultramafic massif is one of the plutonic bodies belonging to the Goiás alkaline province and has a subcircular to ellipsoidal shape, with the ultramafic units (i.e., serpentinized dunite, peridotite, and pyroxenite) in the center of the intrusion and the more differentiated mafic to intermediate products (i.e., alkali gabbros and syenites) at its border. In a few localities, as in Santa Fé, peralkaline and ultrapotassic subvolcanic tabular bodies, such as lamprophyre and phonolite dikes, crosscut the main pluton (Barbour et al., 1979; Brod et al., 2005).

Supergene alteration of the Brazilian ultramafic massifs started during the Eocene to Oligocene and was coincident with the onset of the Sul-Americano geomorphological cycle
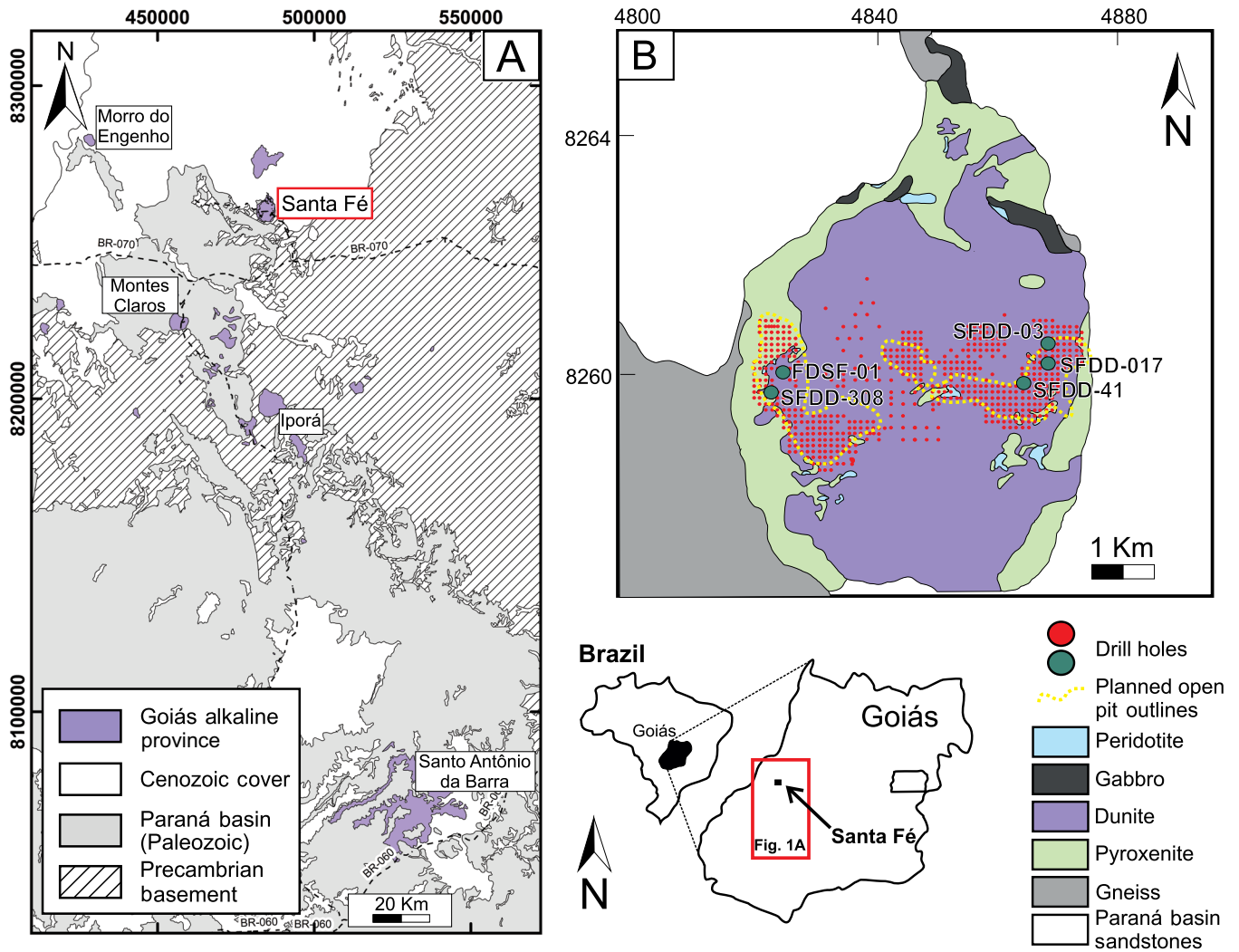
Fig. 1. A) Geologic map of the south Goiás region showing the location of Goiás alkaline province (modified after Lacerda et al., 2000). B) Simplified geologic map of the Santa Fé ultramafic massif (modified after Golightly, 2010) with the drill hole grid. The drill holes used in this work are shown in colors: red circles indicate the location of the drill cores used for the geochemical survey, while the dark green circles show the location of the drill cores sampled for the mineralogical study. Inset map shows location of the study area in the Goiás region.

(Braun, 1971). During this cycle, the main alteration dynamics were silicification under arid to semiarid conditions and lateritization of the ultramafic bodies during warm and humid periods (Melfi et al., 1979). During Miocene-Pliocene, the onset of the Velhas geomorphological cycle led to the dismantling of the Sul-Americano surface and partial reworking and sedimentation of the ancient regolith profiles in the lowlands. Silicified horizons protected the profiles from erosion during the Velhas cycle (de Oliveira et al., 1992, and reference therein). Weathering continues today in the majority of the lateritic districts, with the exception of the São João do Piauì, where the current climatic conditions are arid to semiarid, and mechanical erosion dominates over chemical weathering (de Oliveira et al., 1992).

Local Geology and Laterite Profile

The studied Ni-Co laterite lies upon the ultramafic massif of Santa Fé (Fig. 1B), which consists of a subcircular pluton with an area of about 38 km². The intrusive body comprises a serpentinized dunite core surrounded by peridotite, clinopyroxenite, and minor alkaline gabbro (Barbour et al., 1979; Dreisinger et al., 2008; Golightly, 2010). The laterite cover is mainly located in the flat-lying lowlands, which correspond to the Velhas surface. The remnants of this surface, developed during the Sul-Americano cycle, are still visible and form topographic highs capped by silcrete. De Oliveira et al. (1992) first described the Santa Fé laterite profile as composed of four main horizons and observed that, despite the highest Ni grades being associated with ferruginous saprolite (up to 1.65 wt % Ni), the better-developed and largest ore zone corresponds to the coarse saprolite (minimum Ni content 1.25 wt % NiO). For our study the chemistry and features of the regolith have been analyzed in 613 drill holes and in a number of pits and open cuts, leading to the recognition of eight regolith units within the laterite profile and of three main lithologies in the ultramafic bedrock. The ultramafic bedrock consists of the

following: (1) serpentinized and locally oxidized dunite (lithological code = U1), (2) peridotite (lithological code = U2), (3) pyroxenite (lithological code = U3). The laterite profile is displayed schematically in Figure 2. The thickness of each unit represents the median value taken from the drill holes. The preliminary step in classifying the regolith facies was based on geochemistry, initially defining the oxide- and phyllosilicate-dominated units of the deposit using Mg, recognizing the Mg discontinuity—i.e., the geochemical surface at which Mg phyllosilicates are decomposed in the laterite profile (Freyssinet et al., 2005; Butt and Cluzel, 2013). Further discrimination of regolith units was based on macroscopic features, aimed at recognizing deposit facies affected by mechanical reworking. The laterite profile demonstrates three distinct zones, further subdivided into seven units from bottom to top.

The lowermost zone preserving the original structures and texture of the magmatic parent rock comprises the following: (1) saprock (lithological code = R8), a greenish rock with silica-filled fractures, occurring in all drill cores; its median thickness is 4 m, measured in all drill holes whether they reached bedrock or not, and (2) green saprolite horizon (lithological code = R7, median thickness = 3 m), which is ubiquitous and consists of a brownish to greenish clayey saprolite preserving the original structure of the parent rock. The textures and primary minerals are partly replaced by fine-grained phyllosilicates and oxides.

The ferruginous zones of the profile have been subdivided in two horizons: (3) ferruginous saprolite (lithological code = R6, median thickness = 1.2 m), which is only present in about 50% of drill holes, and (4) ochre saprolite (lithological code = R5, median thickness = 1 m), which occurs only in about 20% of the drill holes and shows the highest Ni grades (mean Ni = 1.44 wt %). The R5 unit marks the transition between saprolite and the ferruginous zones sensu lato. In the ochre saprolite, the original rock features are completely destroyed.

The uppermost ferruginous zones are characterized by reddish hematite-rich layers, subdivided into three further units: (5) a lowermost transition zone (lithological code = R3, median thickness = 0.8 m), comprising a fine-grained and reddish horizon, (6) an overlying indurated ferruginous lateritic crust (lithological code = R2, median thickness = 1.1 m), which has a pisolitic texture with local coatings of Mn oxyhydroxides; this unit has been observed in only about 10% of the drill holes and show the highest Co grades (mean Co = 0.12 wt %), and (7) an uppermost pisolitic topsoil layer (lithological code = R1, median thickness = 3 m) that covers the whole project area. It has a granular texture composed of loose ferruginous pisolites and oolites in a silty to clayey matrix.

Another common lithology is silcrete (lithological code = R4), which consists of an indurated chalcedony-rich layer sporadically occurring on hilltops. The silcrete also occurs as more irregular, discontinuous, and thinner intervals across the regolith units.

Analytical Methods

Mineralogical and petrographic characterization was carried out on 29 samples of the regolith profile collected from selected drill cores (i.e., FDSF-01, SFDD-003, SFDD-017, SFDD-041, SFDD-308; Fig. 1B; App. 1–6). The identification of major minerals was carried out using X-ray powder diffraction (XRPD) analyses, performed with a Panalytical X'Pert PRO MPD diffractometer equipped with an X'celerator PSD 2.1° detector at the Natural History Museum (NHM) in London (UK). The instrument was operated using a Co Kα radiation at 40 kV and 40 mA° with a Fe filter and a 1/4° divergence slit. The XRPD patterns were collected between an incident angle of 5 and 100° 2θ at a step size of 0.02° 2θ. The run time per step was 75 s. The analyses were interpreted with the High Score Plus software, using the PDF-4 database from the International Centre for Diffraction Data (ICDD).
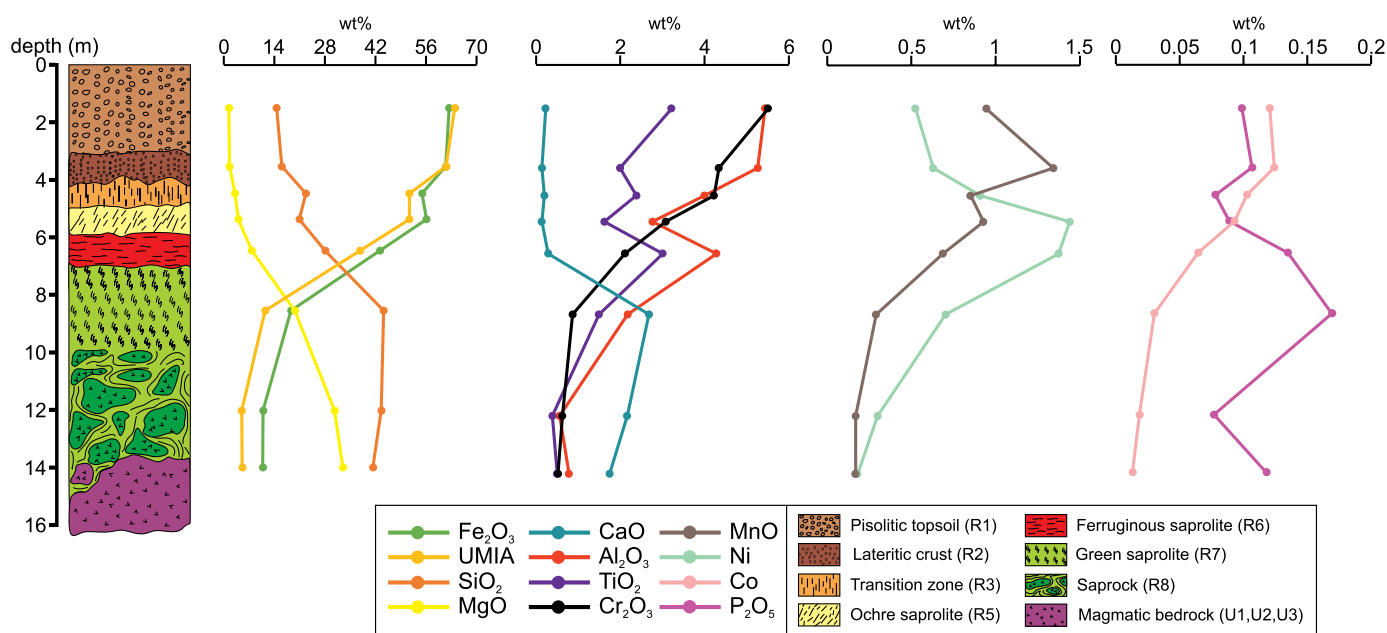

Fig. 2. Schematic section of the Santa Fé laterite profile, based on the considered drill cores and geochemical logs, showing the average chemical composition of each regolith unit.

The study of mineral chemistry of the ore-bearing phases occurring on selected specimens was performed using scanning electron microscopy equipped with energy dispersive X-ray spectroscopy (SEM-EDS) and then refined by electron microprobe analysis (EMPA). SEM-EDS analyses have been carried out at the NHM with a ZEISS EVO LS 15 operating with a working distance of 8.5 mm, an accelerating voltage of 20 kV, and a current of 3 nA. EDS microanalyses were obtained with an X-Max detector. EMPA were performed at the NHM using a Cameca SX100 electron microprobe analyser equipped with five wavelength dispersive spectrometry (WDS) Bragg spectrometers. Peak overlaps corrections were performed prior to matrix correction for the following elements: V (overlapping element: Ti; used standard: RUT STD082), Cr (overlapping element: V; used standard: VAN STDIC), Mn (overlapping element: Cr; used standard: CRO2 STDIC), Fe (overlapping element: Mn; used standard: MNT STDIC). A beam current of 20 nA, an accelerating voltage of 20 keV, and a spot size of 1 μm were used to quantify the following elements: Al (TAP, Kα), Mg (TAP, Kα), P (TAP, Kα), K (PET, Kα), Ca (PET, Kα), Fe (LIF, Kα), Mn (LIF, Kα), Ti (PET, Kα), Co (LIF, Kα), Ni (LIF, Kα), V (LIF, Kα), Cr (PET, Kα), Na (TAP, Kα), Si (TAP, Kα), Cl (PET, Kα), and Zn (PET, Kα).

High-resolution elemental maps were obtained using a FEI Quanta 650 FEG SEM at the NHM. The instrument was equipped with a Bruker Flat Quad 5060F EDS detector for hyperspectral mapping. The maps were acquired at an HV mode and the instrument operated at 15 Kv, with 28-mm working distance and 8-μm pixel time.

The whole-rock geochemical data was treated using multivariate statistical analyses—i.e., principal components analysis (PCA) and factor analysis (FA)—in order to evaluate the associations between the major and minor elements in the laterite profile and to assess the Ni and Co distributions in the different facies of the ore. Combining PCA and FA methods was chosen in order to ensure a much more robust quantitative analysis of geochemical interdependencies (Toffolo et al., 2020). The advantage of PCA is that the number of components is not dependent on the operator's decision, and it is thus effective as an explorative analytical tool. Regarding FA, although the factors produced by this statistical method may be controlled by the user, this will not significantly distort the variance of the data set entirely, resulting in a more reliable result (Reimann et al., 2002, 2011). Therefore, during FA, the approach to the factor extraction was based on (1) the selection of factors with eigenvalues ≥1 and (2) the reduction of the data dimensionality performed by previous PCA (Reimann et al., 2011).

The statistical analyses of the whole-rock geochemical data were conducted on 9,509 samples from ~617 drill holes, provided by Mineradora INVI Ltda. Prior to analysis, each sample was dried at 105°C for 12 h and then crushed to 2 mm. Afterward, a fraction of about 300 g was pulverized in a ring pulverizer to 150 mesh, from which a 10-g portion was selected for whole-rock assays. Major oxides and trace elements were analysed by SGS Geosol Laboratories Ltd. in Belo Horizonte (Brazil), using X-ray fluorescence (XRF). The statistical analyses were performed with the R software. The data were normalized using the isometric log ratio transformation, in or-

der to favor the opening of the data. This transformation requires a matrix of data with no zero. The concentrations below the detection limits have been represented as a multiplication between the detection limit and 0.65 (Martín-Fernández et al., 2003). In order to quantify and to visualize the enrichment of immobile elements (i.e., Fe and Al), as well as the leaching of the mobile components (i.e., Si and Mg) during the weathering process, bulk-rock concentrations were also used for the calculation of the ultramafic index of alteration (UMIA), according to the equation proposed by Babechuk et al. (2014, and references therein):

$$\text{UMIA} = 100 \cdot [(\text{Al}_2\text{O}_3 + \text{Fe}_2\text{O}_{3(T)})/(\text{SiO}_2 + \text{MgO} +$$
$$\text{Al}_2\text{O}_3 + \text{Fe}_2\text{O}_{3(T)})]. \qquad (1)$$

Following the procedure of Aiglsperger et al. (2016, and references therein), the UMIA was calculated with molar ratios by converting into moles the bulk-rock elemental concentrations (wt %).

Results

Geochemistry of the laterite profile

Whole-rock geochemistry: The average chemical composition of the Santa Fé profile's regolith is reported in Figure 2. The dominant oxide in the laterite profile is Fe$_2$O$_3$, (mean ~43.9 wt %), followed by SiO$_2$ (mean ~27.1 wt %) and MgO (mean ~9.7 wt %). The Fe$_2$O$_3$ content increases progressively from the saprock (mean ~10.9 wt %) to the uppermost regolith units (i.e., R6-R1), where it reaches mean concentrations always at or above 50 wt %. SiO$_2$ and MgO show a significant depletion toward the surficial zone of the profile, from a mean of 43.5 wt % SiO$_2$ and 30.7 wt % MgO in the saprock to values around 1.4 wt % SiO$_2$ and 14.5 wt % MgO in the pisolitic soil. Al$_2$O$_3$, Cr$_2$O$_3$ and TiO$_2$ have similar concentrations (~3.5, 2.96, and 2.0 wt %, respectively), while CaO, MnO and P$_2$O$_5$ are very low (~0.83, 0.75, and 0.11 wt %, respectively).

Regarding MgO, a significant drop in its concentration was observed at the transition between green and ferruginous saprolite. A slight increase in the MnO concentration is observed at the transition between the green saprolite (~0.29 wt %) and the uppermost section of the ore zone (i.e., R6-R1, mean >~0.60 wt %), with the highest MnO concentration occurring in the lateritic crust (~1.43 wt %). In the regolith profile, Ni and Co have mean concentrations ~0.84 and 0.08 wt %, respectively, with the highest Ni grades occurring in the ferruginous and the ochre saprolite horizons (mean 1.3 and 1.4 wt %, respectively). The Co grade is negligible in the saprock and in the green saprolite (mean < 0.05 wt %), while it is higher in the surficial regolith (0.06–0.12 wt %). The dominant oxide in the silcrete unit is SiO$_2$ (~64.6 wt %), followed by MgO and Fe$_2$O$_3$ (mean ~16.5 and 11.4 wt %, respectively). The Ni and Co grades measured in the silcrete are significantly lower (~0.3 and 0.04 wt %, respectively), in comparison with the other regolith units (Table 1).

The saprock and the green saprolite units have the lowest UMIA (Figs. 2, 3; Table 1) (~4.9 and 11.4, respectively), whereas the samples from the ferruginous saprolite to the pisolitic topsoil (R6-R1) show a significant increase in the UMIA (up to 63.9 in the R1 unit), due to the enrichment of Al$_2$O$_3$ and Fe$_2$O$_3$ in the uppermost zones of the profile. As ex-

Table 1. Average Chemical Composition (wt %) of the Santa Fé Laterite Regolith Units (R8-R1[1]), the Magmatic Bedrock (U1, U2, U3), and the Silcrete Horizon (R4)

	SiO_2	Al_2O_3	MgO	MnO	Fe_2O_3	TiO_2	P_2O_5	CaO	Cr_2O_3	Co	Ni	UMIA
Avg regolith units (R8-R1)1	27.16	3.5	9.74	0.75	43.93	2.01	0.11	0.83	2.96	0.08	0.84	N/A
Avg dunite (U1)	40.6	0.34	34.77	0.17	10.99	0.23	0.04	0.62	0.51	0.01	0.21	4.57
Avg peridotite (U2)	41.38	0.13	36.07	0.16	9.68	0.13	0.04	0.34	0.66	0.01	0.19	3.81
Avg pyroxenite (U3)	41.95	1.88	28.08	0.18	11.67	1.15	0.27	4.28	0.39	0.01	0.14	6.88
Avg bedrock (U1, U2, U3)	41.31	0.78	32.97	0.17	10.78	0.5	0.12	1.75	0.52	0.01	0.18	N/A
Avg silcrete (R4)	64.67	0.71	16.51	0.19	11.47	0.36	0.09	0.24	0.78	0.04	0.34	5.59

[1]The silcrete horizon is not included in the calculation

pected, the silcrete unit has a low UMIA (5.5), characterized by a progressive trend toward elevated SiO_2 content. Despite the general rise of the UMIA in the oxyhydroxide-dominated zones of the orebody (R6-R1), the Fe_2O_3 and Al_2O_3 increase in these zones is not accompanied by a total MgO loss. In fact, some compositions measured in the R6, R5, and R3 are displaced toward more MgO-rich compositions in comparison with the typical in situ lateritization trend observed in other deposits (e.g., Wingellina, Putzolu et al., 2019; Moa Bay, Aiglsperger et al., 2016). The UMIA does not show any relationship with the Ni grades, while a slight covariance between Co

and UMIA is observed in samples from the ferruginous saprolite to the pisolitic topsoil (Fig. 4). However, the highest Co concentrations (>0.20 wt % Co) fall outside the correlation trends, giving rise to outliers.

Principal component analysis: To visualize the interelemental relationships, a PCA has been carried out on the bulk-rock chemical assays, firstly taking into account all the major and minor oxides, together with Ni and Co (Fig. 5A), and secondly selecting only MnO, Cr_2O_3, Fe_2O_3, SiO_2, Ni, and Co (Fig. 5B-E).

In the first PCA (Fig. 5A; App. 7), the first two components explain ~71% of the total variance (52.3% PC1 and 19.3% PC2)
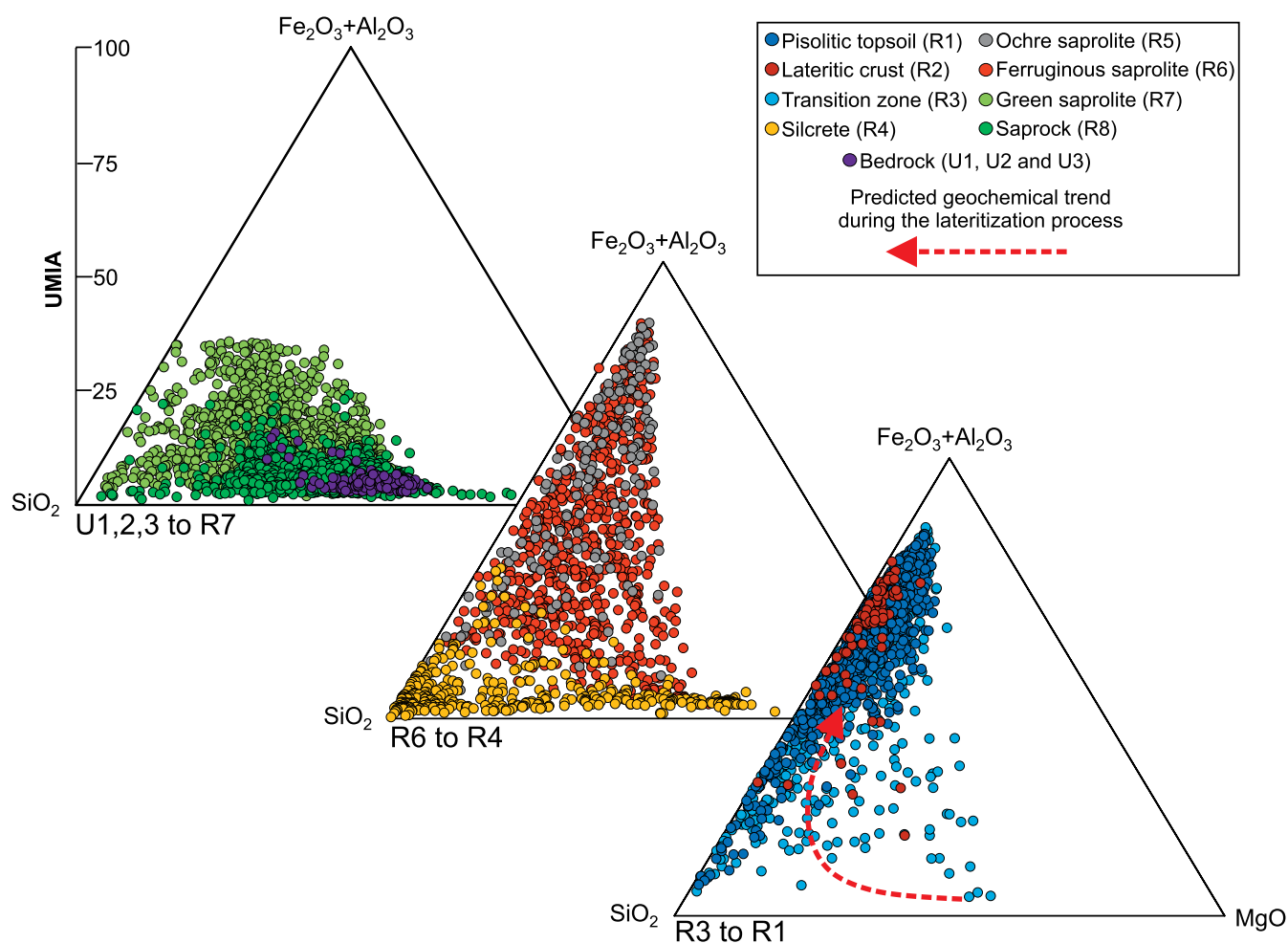

Fig. 3. $MgO-SiO_2-(Al_2O_3 + Fe_2O_3)$ molar ternary plot, showing the geochemical variations in the Santa Fé deposit during chemical weathering. The UMIA has been calculated following the equations of Babechuk et al. (2014) and Aiglsperger et al. (2016).
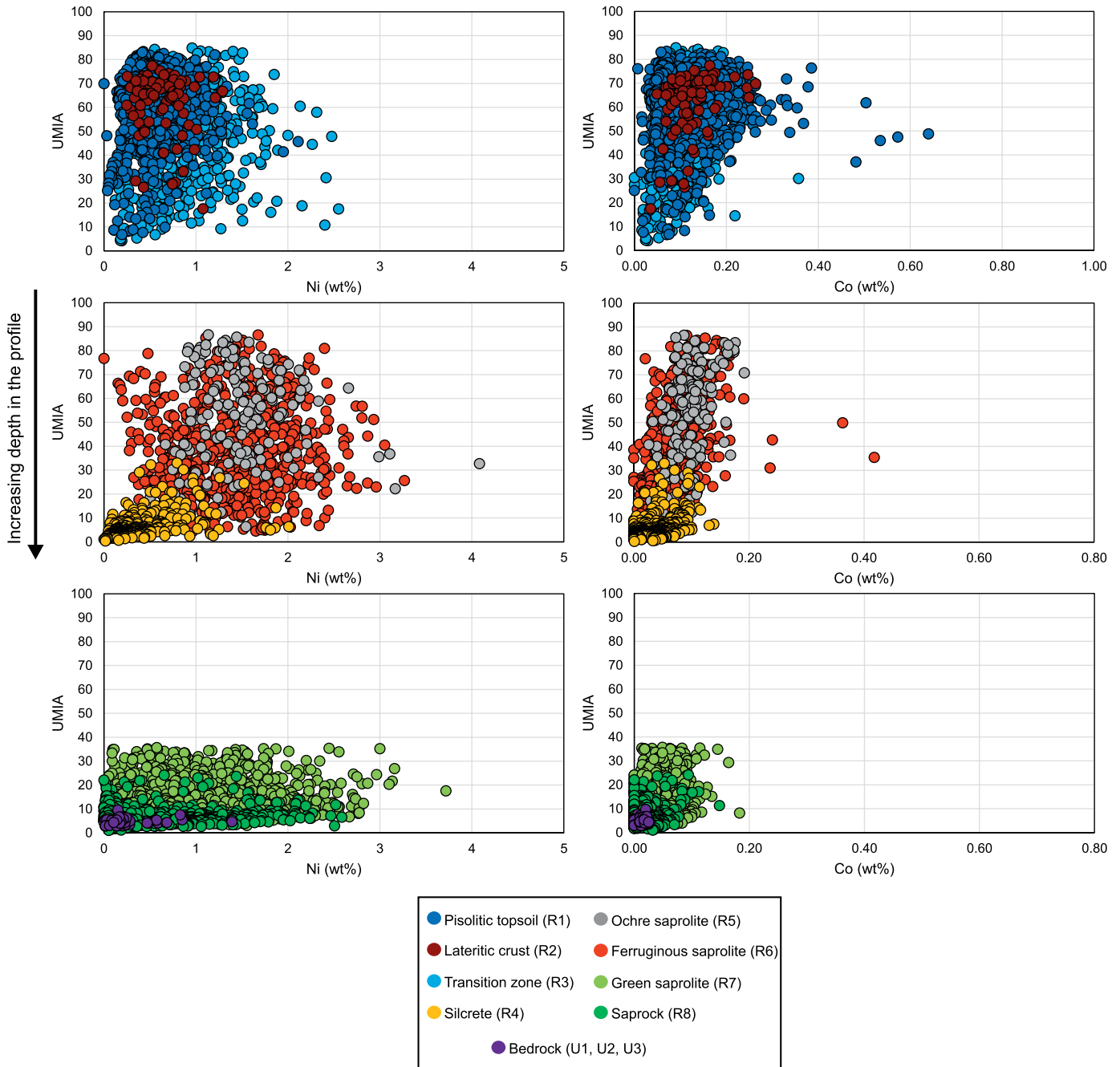
Fig. 4. Binary plots showing the relationship between the metal grades and the UMIA.

of the geochemical data set. Along the PC1 axis, the MgO and the SiO₂ eigenvectors show a positive correlation toward negative PC1 values. They form an anticorrelated group with Fe_2O_3-MnO and are relatively less anticorrelated with TiO_2-Al_2O_3-Co-Cr_2O_3-Ni, which have variably positive and negative PC2 values. However, PC1 was able to discriminate the (phyllo)silicate- and oxide-dominated sections of the orebody (bedrock samples to ochre saprolite and silcrete; ferruginous saprolite to pisolitic topsoil, respectively). Along the PC2 axis, Al_2O_3 and TiO_2 show a good correlation in the R6 to R1 units, while CaO and P_2O_5 are significantly displaced toward higher PC2 values and are correlated within the lower section of the

profile (U-R7). The MnO, Co, Cr_2O_3 and Ni eigenvectors display a progressive displacement toward negative PC2 values and are mostly distributed within oxide-dominated sections of the ore. The PCA of the full data set highlighted a complex Co deportment, which is associated with a relatively wide group of elements (mostly Cr_2O_3-Mn and less Ni-Fe_2O_3). Therefore, the second PCA was conducted on selected variables to better constrain the Co behavior (Fig. 5B-E; App. 8). In this PCA, PC1 explains ~67% of the total variance, PC2 accounts for 14%, and the components that are subsequent to PC2 account for significant proportions of the bulk variance. In the PC1 versus PC2 plot (Fig. 5B) Co is closely associated with
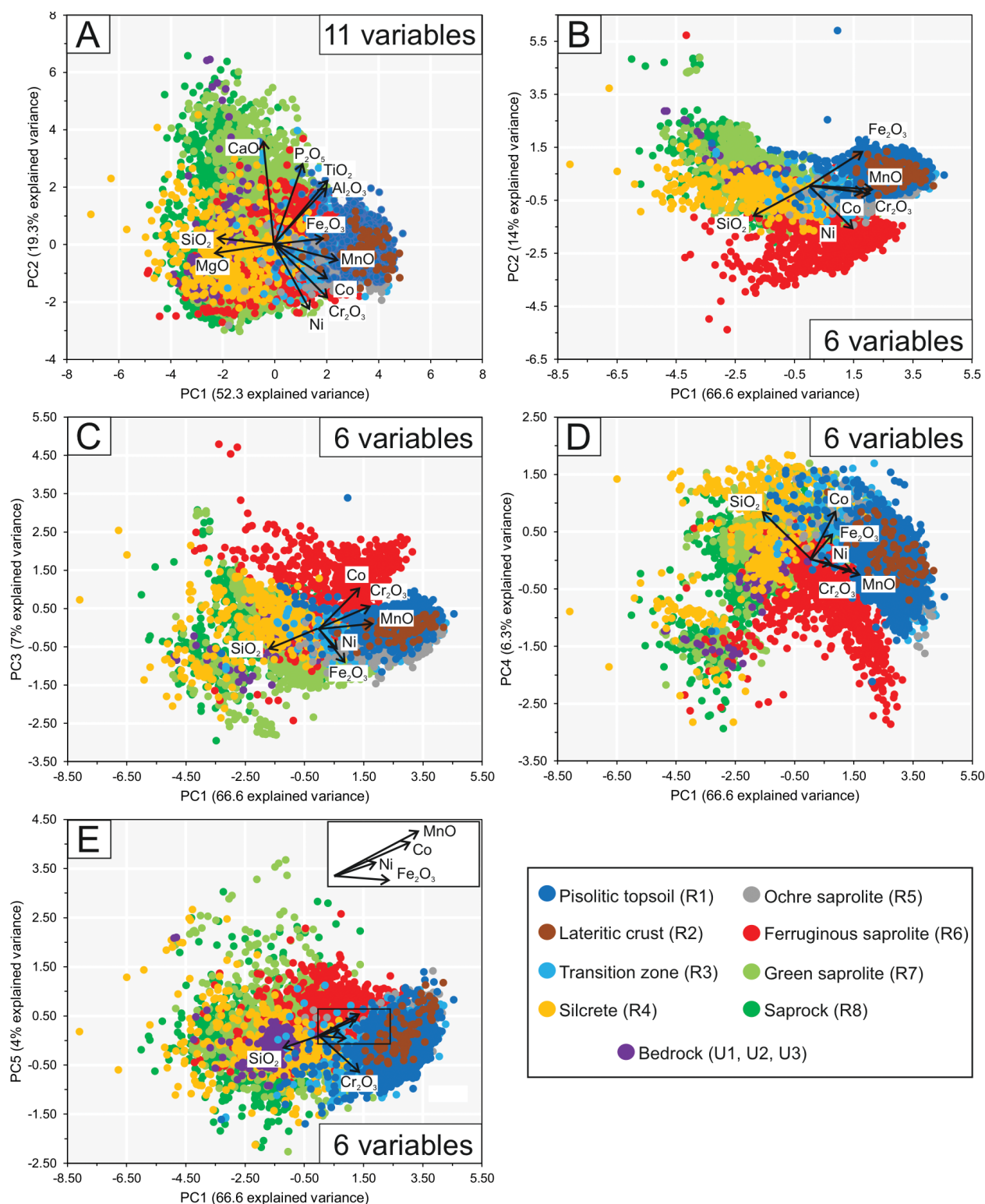
Fig. 5. A) PC1 versus PC2 biplot showing the association between the major and minor oxides in the Santa Fé geochemical data set. B-E) PC1 versus PCn biplot showing the association of Ni and Co with MnO, Cr_2O_3, and Fe_2O_3 and SiO_2.

MnO and Cr_2O_3 (R1, R2, R3, and R5 units), while Ni (R6 unit) and Fe_2O_3 (R1 unit) are displaced toward negative and positive PC2 values, respectively. The Co-Cr_2O_3-Mn group is dominant also in the PC1 versus PC3 plot (Fig. 5C), but here

Co is slightly decoupled toward positive PC3 values. In addition, Ni and Fe_2O_3 are strongly correlated with negative PC3 values. The PC1 versus PC4 plot shows a similar scenario, with a correlation between Co and Fe_2O_3 along positive PC4

values and a strong association between MnO, Ni, and Cr_2O_3. Lastly, the PC1 versus PC5 (Fig. 5E) plot is the only computation where Cr_2O_3 is decoupled from the other variables, which form the Fe_2O_3-Ni-Co-MnO group characterized by low to moderately positive PC5 values.

Factor analysis: A factor analysis (after Varimax rotation) has been performed on each regolith unit and on the magmatic bedrock (App. 9). The MnO-Fe_2O_3-Co-Cr_2O_3 group, showing positive weightings, is widespread in almost the whole data set (i.e., in the magmatic bedrock and in the R8, R7, R5, R4, and R3 units) and occurs in the first factor in association with the SiO_2 and MgO pair, which is instead characterized by negative loadings. These groups collectively account for 20 to 34% of the explained variance. The association between MnO-Fe_2O_3-Co-Cr_2O_3 becomes more complex in the lateritic crust, in the pisolitic topsoil, and to a lesser extent in the ochre saprolite horizons. In the former, Fe_2O_3 shows a positive weighting in association with negative weightings of SiO_2 and MgO in F1, while MnO and Co are positively correlated with Al and Ni in F2. In this context, Cr is geochemically decoupled and shows a positive weighting in F3. In the pisolitic topsoil, Fe_2O_3 occurs in F1, while the F4 and F5 factors highlight the Mn-Ni-Co and Cr-Co associations, respectively. Although the Cr-Co association occurs in the last factor (F5), it accounts for 9% of the explained variance. The Cr-Co association, accounting for 10% of the total variance, has been detected also in the F3 of ochre saprolite unit. Other important associations are the Al_2O_3-TiO_2-CaO-P_2O_5 group, occurring throughout the profile, and Ni-Mg (and locally TiO_2-Al_2O_3-Fe_2O_3), which have been detected from the ferruginous and ochre saprolites and in the pisolitic topsoil.

Mineralogy and textures

X-ray powder diffraction (Fig. 6) shows that the saprock unit consists of remnant magmatic olivine and pyroxene, of layered silicates (i.e., chlorite, serpentine, and vermiculite), together with spinel group minerals. The mineralogy of the green saprolite is similar to that of the saprock, except that it also contains smectite. In the uppermost units of the laterite profile (R6 to R1), goethite, hematite and magnetite are the dominant oxyhydroxides, while chlorite is the only phyllosilicate. Mn oxyhydroxides have been also detected and occur as minor constituents of the ore.

In the saprock, olivine is crosscut by several generations of serpentine with typical mesh-like textures (Fig. 7A), while pyroxenes are cut by veinlets of serpentine and/or cryptocrystalline quartz (Fig. 7B, C). In the green saprolite, newly formed serpentine has totally obliterated the magmatic texture; it occurs in two generations: massive (srp I) and vein-filling (srp II) serpentine (Fig. 7D). Chlorite occurs extensively in the saprock and green saprolite units, either as filling of cavities in cryptocrystalline silica (Fig. 7E) or as replacement of spinels (Fig. 7F). Smectite clays only occur as alteration rims around olivine in the phyllosilicate-dominated section of the profile (Fig. 7F). Remnants of perovskite and apatite occur extensively mostly in the lowermost section of the profile (Fig. 7H, I), with the former commonly exhibiting Al-bearing Ti oxide alteration rims (Ti/Al oxide I, Fig. 7H).

Hypogene Cr-Fe oxides (chromite, ferritchromite, and magnetite) are abundant throughout the whole laterite pro-

file. Based on its texture, two types of magnetite were detected: coarse-grained magnetite I (mt I) (Fig. 8A), which commonly shows either hematite lamellae (hem I, martitization, Fig. 8B) or ilmenite exsolutions (Fig. 8C), or magnetite II (mt II), which mainly occurs in the saprock and in the green saprolite as tiny rims around serpentine (Fig. 7A-D). Chromite commonly shows porous/spongy alteration zones that are locally spread toward the grain core, thus indicating a pervasive alteration of the Cr spinel (Fig. 8D). Two ferritchromite (Fe-chr) generations were also recognized, with Fe-chr I occurring as massive grains, which host amphibole and Ni-Fe(Co) sulfide inclusions (Fig. 8E). Furthermore, a late generation of zoned ferritchromite (Fe-chr II) was observed partially replacing Fe-chr I (Fig. 8F).

Among newly formed Fe oxyhydroxides, a first type of goethite (ght I) occurs as skeletal aggregates in the lowermost section of the profile (i.e., saprock and green saprolite, Fig. 9A). The textures of the more surficial ferruginous saprolite show a certain degree of reworking, with ubiquitous composite Fe oxyhydroxide-rich oolites (Fig. 9B) and detrital chlorite (Fig. 9C). Supergene hematite (hem II) is commonly found in the core of the ooids, while goethite occurs at their external rims (Fig. 9B). Hematite locally occurs also as massive crusts (Fig. 9D). Late generations of Ti and Al oxyhydroxides have been extensively detected: a second generation of Ti/Al oxide (Ti/Al oxide II) was observed as globular and concentric aggregates (Fig. 9E). Veinlets of gibbsite cutting the hematite/goethite ooids have been observed (Fig. 9F). Mn hydroxides occur in the lowermost section of the profile as replacement of chlorite (Fig. 9G, H), while in the oxide-dominated units they form massive to layered encrustations (Fig. 9I).

Mineral chemistry

Selected microprobe analyses of ore-bearing and gangue minerals are reported in Tables 2 to 7, while box and whisker plots, showing the full data sets in chemical variance of the pre-lateritic and the supergene phases are reported in Appendixes 10 and 11, respectively.

Ferromagnesian minerals: Forsteritic olivine (Fo# mean = 87.56) has average Ni and Co contents of 0.35 wt % NiO and 0.03 wt % CoO, respectively. Clinopyroxene (diopside) and amphibole (K-bearing ferropargasite) have very low Co (mean CoO = 0.03 wt % and below detection limit, respectively) and Ni grade contents (mean NiO = 0.17 wt % and below detection limit, respectively).

Prelateritic Fe-Cr oxides: Chromite displays significant amounts of Cr, Fe^{2+}, Al, Mg, and Ti (mean = 50.61 wt % Cr_2O_3, 19.69 wt % FeO, 7.99 wt % Al_2O_3, 7.49 wt % MgO, and 2.88 wt % TiO_2). In a limited group of analyses, chromite grains are also enriched in Fe^{3+} (up to 14.36 wt % Fe_2O_3), indicating an incipient transformation to Fe^{3+}-bearing chromite (ferritchromite). In ferritchromite I, Fe is the dominant element, while the Cr amounts are relatively low (mean = 39.82 wt % Fe_2O_3, 26.05 wt % FeO, and 23.91 Cr_2O_3). Minor concentrations of Ti, Al, Mg, and Zn have been also detected (mean = 3.62 wt % TiO_2, 1.08 wt % Al_2O_3, and 4.10 wt % MgO, 1.54 wt % ZnO). In comparison with ferritchromite I, ferritchromite II displays higher Al, Cr, and Zn concentrations (mean = 5.57 wt % Al_2O_3, 39.51 wt % Cr_2O_3, and 12.16 wt % ZnO, respectively) and lower Fe^{3+} concentra-
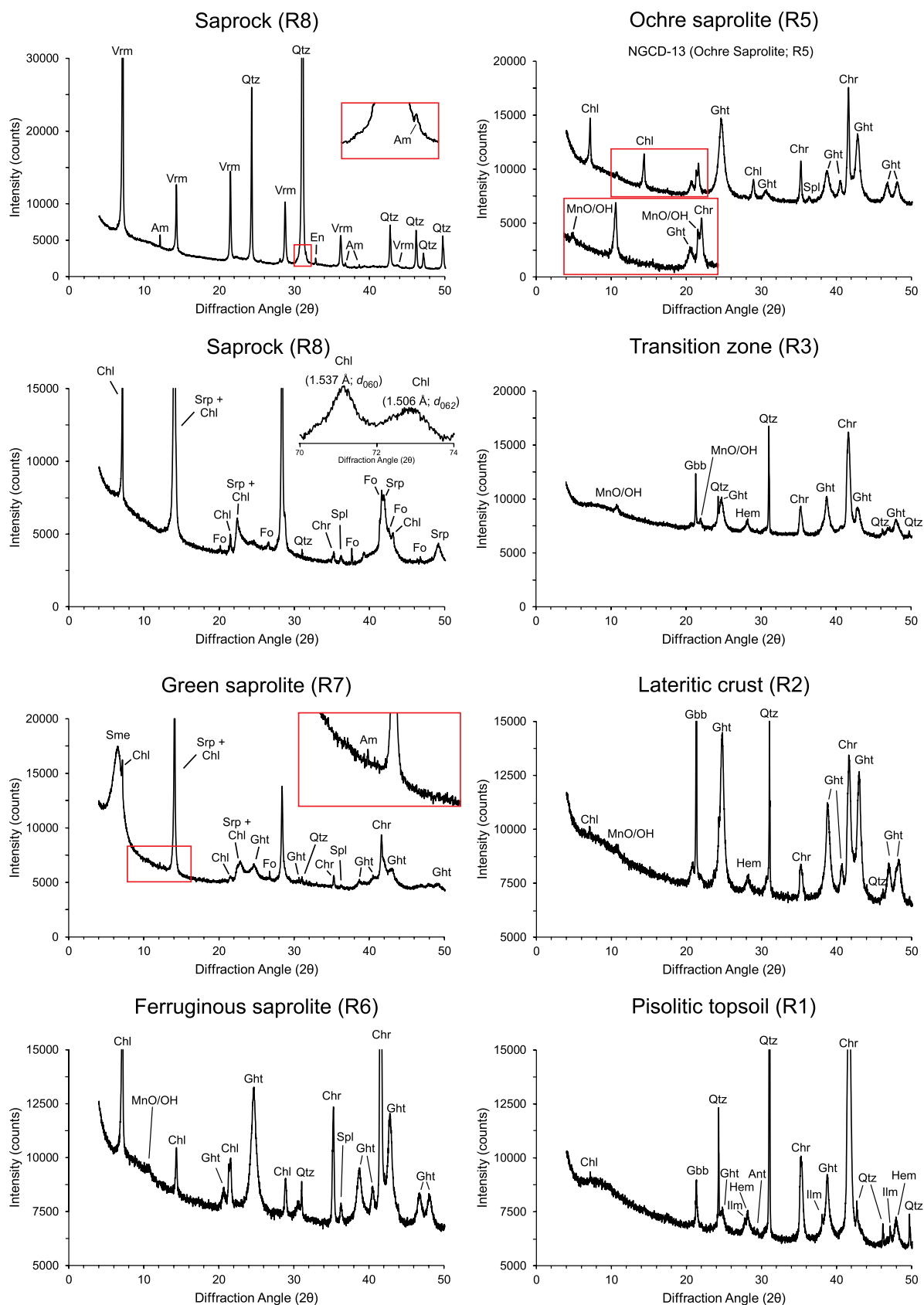
Fig. 6. Representative XRPD patterns of the regolith units in the Santa Fé laterite. Mineral abbreviations: Am = amphibole, Ant = anatase, Chl = chlorite, Chr = chromite, En = enstatite, Fo = forsterite, Gbb = gibbsite, Ght = goethite, Hem = hematite, Ilm = ilmenite, MnO/OH = Mn oxyhydroxide, Qtz = quartz, Sme = smectite, Spl = spinel, Srp = serpentine, Vrm = vermiculite.
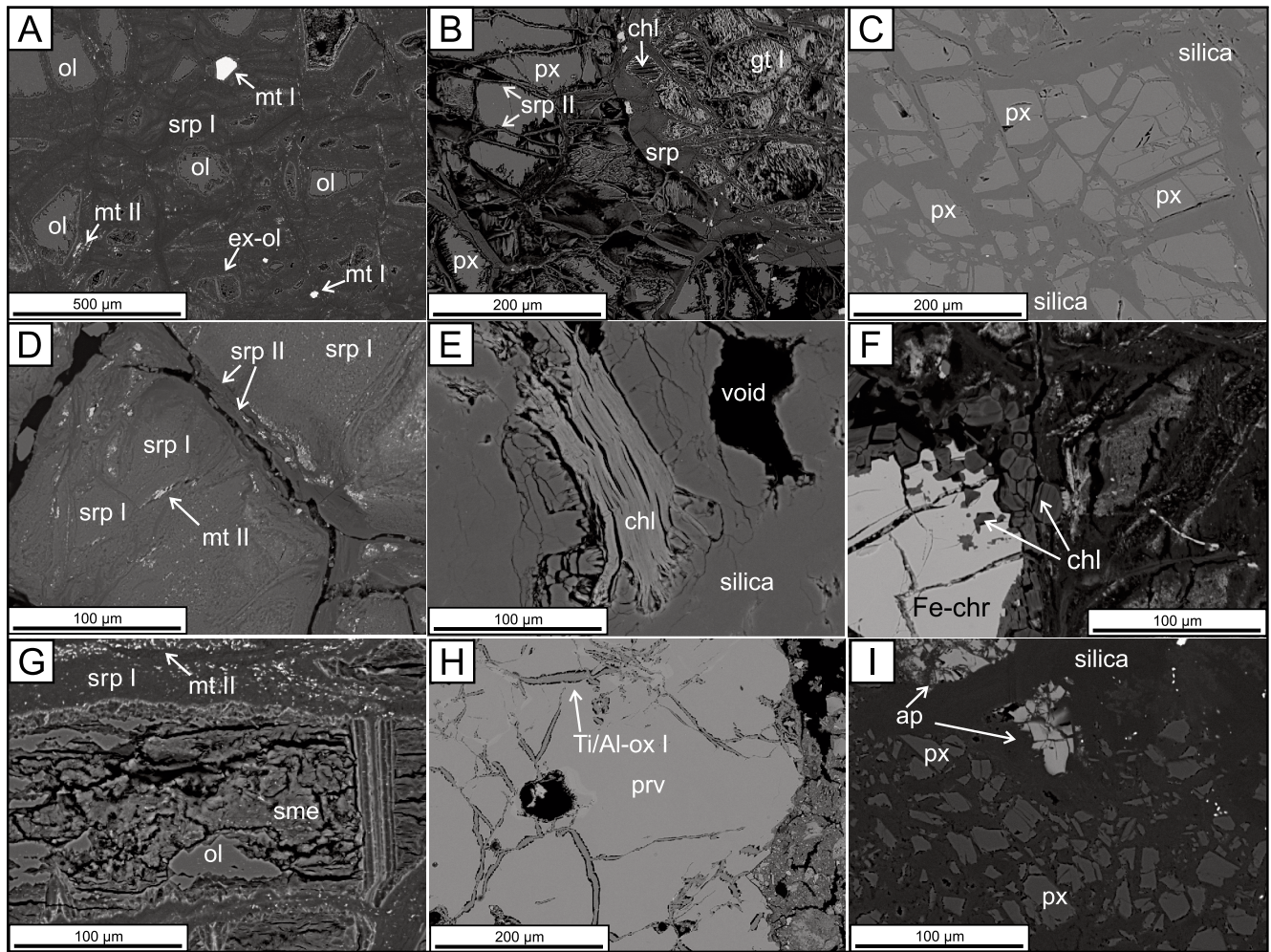
Fig. 7. Backscattered electron photomicrographs showing the typical textures of the magmatic minerals and of the newly formed phyllosilicates. A) Serpentine and magnetite II enveloping olivine grains (saprock). B) Mesh of serpentine replacing pyroxene grains (saprock). C) Cryptocrystalline quartz cementing pyroxene (saprock). D) Mesh serpentine II crosscutting pseudomorph serpentine I (green saprolite). E) Layered chlorite within cryptocrystalline silica. F) Newly formed chlorite replacing a spinel grain (green saprolite). G) Pelitomorphic smectite replacing olivine. H) Primary perovskite grains crosscut by Ti/Al-oxide I (transition zone). I) Apatite and pyroxene grains cemented by cryptocrystalline silica (saprock). Mineral abbreviations: ap = apatite, chl = chlorite, chr = chromite, ex-ol = ex olivine, Fe-chr = ferritchromite, gt = goethite, mt = magnetite, ol = olivine, prv = perovskite, px = pyroxene, sme = smectite, srp = serpentine, Ti/Al-ox = Ti/Al-oxide.

Table 2. Chemical Composition (wt %) of Selected Ferromagnesian Minerals

| Oxides	Olivine		Clinopyroxene		Amphibole	
Na$_2$O	0.04	0.00	0.27	0.38	5.61	5.31
MgO	46.19	45.61	16.68	16.53	21.62	21.82
Al$_2$O$_3$	0.00	0.08	1.10	1.23	0.15	0.09
SiO$_2$	37.97	37.80	53.40	53.27	54.89	53.91
K$_2$O	0.02	-	-	-	2.63	2.58
CaO	0.14	0.08	24.79	25.28	6.69	6.65
TiO$_2$	-	0.03	0.98	1.05	1.10	1.08
Cr$_2$O$_3$	-	0.00	0.63	0.92	0.04	-
MnO	0.27	0.21	0.04	0.01	-	0.06
FeO$_t$	11.42	11.08	3.92	3.67	1.96	2.02
CoO	0.01	0.08	0.08	-	0.05	0.03
NiO	0.33	0.41	0.25	0.17	0.06	0.17
Fo#	87.82	88.01	-	-	-	-
Total	96.41	95.38	102.14	102.51	94.81	93.72

Notes: - = not detected
Fo = forsterite
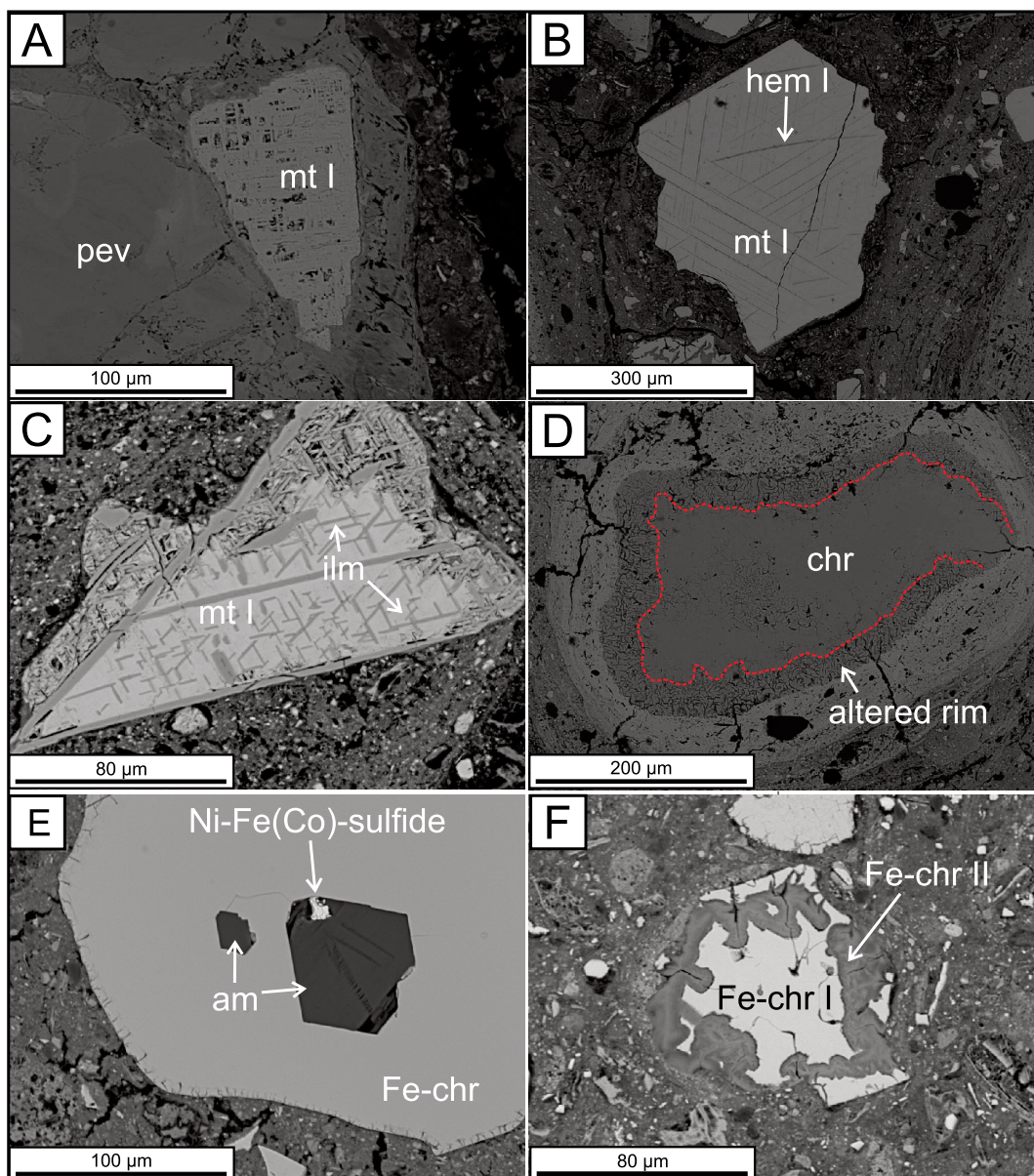
Fig. 8. Backscattered electron photomicrographs showing the typical textures of the spinels. A) Coarse magnetite I grain associated with partially altered perovskite. B) Magnetite I grain exhibiting hematite exsolutions (hem I; martitization) (transition zone). C) Magnetite I with trellis-type ilmenite exsolutions (ferruginous saprolite). D) Chromite grain with pervasive alteration rim (transition zone). E) Ferritchromite I enclosing amphibole and Ni-Fe(Co) sulfide inclusions (transition zone). F) Ferritchromite II replacing ferritchromite I (ferruginous saprolite). Minerals abbreviations: am = amphibole, chr = chromite, Fe-chr = ferritchromite, hem = hematite, ilm = ilmenite, mt = magnetite, pev = perovskite.

tions (mean = 6.21 wt % Fe_2O_3). Iron is the main cation in magnetite (mean = 69.83 wt % Fe_2O_3 and 34.74 wt % FeO), which locally exhibits relatively high Ti and Al amounts (up to 8.56 wt % TiO_2 and 3.25 wt % Al_2O_3). Moreover, the Fe-Cr oxides contain traces of Ni, Co, and Mn. There are significant amounts of Co in the chromite grains (up to 0.53 wt % CoO), whereas their Ni content is lower (<0.20 wt % NiO) and is similar to that of ferromagnesian minerals. High Ni and Co contents were measured in ferritchromite. Ferritchromite I has Ni and Co concentrations up to 1.94 wt % NiO and 1.63 wt % CoO, while in ferritchromite II the Ni and Co grades reach values up to 2.29 wt % NiO and 1.23 wt % CoO.

Manganese occurs as a minor element mainly in chromite and ferritchromite I (up to 1.73 and 1.41 wt % MnO).

Other significant chemical features of Fe-Cr oxides can be observed on the Al-Cr-Fe^{3+} projection of the spinel prism (Fig. 10). In particular, the analyzed minerals are characterized by a progressive chemical evolution between the chromite and magnetite end members, following an increase of Fe^{3+} (Fig. 10A). Interestingly, in the Al-Cr-Fe^{3+} system (Fig. 10B) the analyzed primary chromite plots within the very low grade metamorphic field (i.e., greenschists facies), while most of the ferritchromite data are spread within the metamorphic field ranging from lower to upper amphibolite fa-

Table 3. Chemical Composition (wt %) of Selected Fe-Cr Oxides

Oxides	Chromite		Ferritchromite I		Ferritchromite II		Magnetite	
Na_2O	0.16	0.17	0.05	-	-	0.35	-	0.01
MgO	0.4	0.53	3.57	3.67	0.44	0.21	0.06	-
Al_2O_3	8.88	7.34	0.01	1.18	5.16	5.08	2.56	3.15
SiO_2	1.19	0.94	0.05	0.03	4.14	4.91	1.13	0.89
K_2O	0.01	0.01	-	-	-	0.05	0.09	-
CaO	-	-	0.11	0.09	0.41	0.23	0.03	-
TiO_2	2.85	2.6	5.64	3.76	2.03	2.29	2.6	0.42
Cr_2O_3	62.93	58.33	13.94	17.87	39.25	40.49	0.62	0.35
MnO	1.72	1.88	0.59	0.27	0.06	-	-	0.28
Fe_2O_3	-	-	45.27	43.57	7.58	6.1	57.87	61.66
FeO	20.99	26.25	25.83	24.8	23.16	24.14	34.45	32.14
CoO	0.52	0.52	1.63	1.25	1.23	0.7	0.4	0.26
NiO	0.11	0.12	0.48	0.45	1.35	1.9	0.2	0.28
ZnO	-	-	2.26	2.68	13.75	12.51	-	-
Tot	99.77	98.7	97.17	96.93	84.81	86.44	100.02	99.45
Cr/[Cr+Al]	0.83	0.84	1	0.91	0.84	0.84	0.14	0.07
$Fe^{2+}/[Fe^{2+}+Fe^{3+}]$	1.6	1.23	0.39	0.39	0.77	0.81	0.4	0.37
$Fe^{3+}/(Fe^{3+}+Fe^{2+})$	0	0	0.61	0.61	0.23	0.19	0.6	0.63
$Mg/[Mg+Fe^{2+}]$	0.03	0.03	0.2	0.21	0.03	0.02	0	0

Notes: Fe^{2+} and Fe^{3+} by stoichiometry; - = not detected

cies. This is also confirmed by the data distribution in the cross plot of Figure 10C, where ferritchromites (I and II), as well as a few chromite analyses, show Cr and Mg numbers (i.e., Cr/[Cr + Al] and $Mg/[Mg + Fe^{2+}]$, respectively) different from the conventional mantle spinels, being instead located in the high-temperature compositional field of altered spinels observed in other ultramafic suites (Arai and Akizawa, 2014, and reference therein). Another relevant aspect is shown by the geochemical transect performed in a residual chromite grain, which exhibits a well-developed reaction rim (Fig. 10D). The main chemical variations between the fresh chromite core and the altered rim are the decrease of the Cr, Mg, and Al concentrations and the increase of the total Fe content (Fe^{2+} and Fe^{3+}).

Mg-Ni phyllosilicates: The chemistry of mesh-like (srp I) and vein-filling (srp II) serpentine is characterized by very similar Mg contents (mean = 34.38 and 32.49 wt % MgO respectively), while Ni, Fe, and Al differ significantly among the two serpentine generations. In srp I, Al, Fe, and Ni are relatively low (mean = 0.49 wt % NiO, 7.80 wt % FeO_t, and 0.17 wt % Al_2O_3), while in srp II Al (mean = 0.74 wt % Al_2O_3) as well as Ni and Fe are significantly increased (1.64 wt % NiO and 11.08 wt % FeO_t). In smectite clays the octahedral site is characterized by high Mg and Fe contents (mean = 16.89 wt % MgO and 12.16 wt % FeO_t), while Al and Ni occur as minor cations (mean = 1.88 wt % Al_2O_3 and 1.54 wt % NiO). Chlorite contains variable amounts of Ni (0–11.50 wt % Ni, mean = 3.04 wt % Ni). Overall, Mg is the dominant octahedral cation (mean = 23.61 wt % MgO), followed by Al and Fe (mean = 9.06 wt % Al_2O_3 and 7.35 FeO_t). Furthermore, chlorite contains variable amounts of Ti and Cr, which can reach concentrations up to ~5 wt % TiO_2 and 1 wt % Cr_2O_3.

Secondary oxyhydroxides: Among Mn oxyhydroxides, three mineral species have been identified at Santa Fé: romanèchite, asbolane, and lithiophorite-asbolane intermediates. Overall, Co is almost equally distributed within Mn oxyhydroxides, with romanèchite showing a slight enrichment (mean = 3.62 wt % CoO) in comparison with asbolane and

lithiophorite-asbolane (mean = 2.58 and 2.35 wt % CoO, respectively). Nickel is rich in asbolane (mean = 20.20 wt % NiO), and to a lesser extent in romanèchite and lithiophorite-asbolane (13.16 and 12.43 wt % NiO, respectively). Barium is a major constituent of romanèchite (mean = 5.13 wt % BaO), whereas lithiophorite-asbolane shows high Al concentrations (12.32 wt % Al_2O_3). In the Al-Ni-Co system (Fig. 11), the chemistry of Mn oxyhydroxides from Santa Fé is significantly different from those of other world-class Co-bearing laterite deposits, such as Wingellina (Western Australia; Putzolu et al., 2018) and Nkamouna (southeast Cameroon; Lambiv Dzeuma et al., 2013). In particular, despite the observation that Mn oxyhydroxides have high Ni concentrations, the Co grades are significantly lower in comparison with the above-mentioned deposits. Hematite has average Ni and Co contents of 0.80 wt % NiO and 0.23 wt % CoO, while goethite is more Ni rich (mean = 0.97 wt % NiO) and has a lower Co grade (mean = 0.18 wt % CoO).

To better constrain the elements deportment in Fe and Mn oxyhydroxide-bearing zones of the ore, energy dispersive X-ray microanalysis (EDX) high-resolution maps were carried out on selected hydroxide-rich regions of the ferruginous saprolite (R6; Fig. 12), where relict skeletal goethite is coated

Table 4. Chemical Composition (wt %) of Selected Ti Oxides

Oxide	Ilmenite		Ti/Fe-Al oxide		Perovskite	
Na_2O	-	0.11	0.24	0.05	0.73	0.57
MgO	8.3	2.59	0.18	-	-	0.09
Al_2O_3	0.01	0.24	8.29	6.21	0.06	0.13
SiO_2	0.01	0.13	0.91	0.86	0.02	-
K_2O	-	-	0.03	-	0.07	0.1
CaO	-	-	-	0.02	38.68	38.93
TiO_2	54.62	46.9	86.24	88.53	56.46	56.23
Cr_2O_3	0.06	0.22	0.1	0.29	-	-
MnO	0.71	1.87	0.17	0.02	-	-
FeO_t	35.68	47.35	2.78	2.89	0.66	1.24
CoO	0.03	0.15	-	0.08	0.24	-
NiO	0.03	0.11	0.09	0.08	0.21	0.12
Total	99.46	99.67	99.03	99.02	98.9	99.76

Notes: - = not detected

Table 5. Chemical Composition (wt %) of Selected Mg-Ni Phyllosilicates

Oxides	Serpentine I		Serpentine II		Smectite		Chlorite		
Na_2O	-	0.01	-	-	-	-	-	0.03	0.08
MgO	37.04	37.46	31.82	31.12	20.78	22.72	20.43	20.01	23.2
Al_2O_3	0.64	0.47	0.83	0.85	2.87	2.65	15.15	16.02	12.7
SiO_2	40.99	39.53	37.52	37.89	50.74	55.22	30.87	30.57	37.82
K_2O	-	-	-	0.04	0.08	0.05	0.02	-	-
CaO	0.11	0.06	0.06	0.14	0.28	0.14	-	-	0.01
TiO_2	0.12	0.03	0.05	0.32	0.15	0.23	1.63	1.58	5.22
Cr_2O_3	0.07	0.1	0.16	0.12	0.7	0.77	0.15	0.13	1.14
MnO	0.04	0.05	0.21	0.22	0.01	0.05	0.04	-	0.09
FeO_t	8.88	8.66	12.8	14.4	6.69	7.26	4.79	4.48	5.3
CoO	-	0.1	0.25	0.14	0.08	0.14	0.04	-	-
NiO	1.07	1.03	2.18	2.07	2.2	2.27	11.5	11.49	1.08
Total	88.96	87.52	85.87	87.3	84.59	91.49	84.63	84.32	86.65
	a.p.f.u. on the basis of $O_5(OH)_4$				a.p.f.u. on the basis of $O_{10}(OH)_2$		a.p.f.u. on the basis of $O_{10}(OH)_8$		
Si	1.95	1.92	1.92	1.92	3.81	3.83	3.2	3.17	3.59
Al^{IV}	0.04	0.03	0.05	0.05	0.19	0.17	0.8	0.83	0.41
Fe^{IV}	0.01	0.05	0.03	0.03	-	-	-	-	-
Sum_{Tet}	2	2	2	2	4	4	4	4	4
Al^{VI}	-	-	-	-	0.07	0.05	1.06	1.13	1.02
Fe^{VI}	0.34	0.3	0.51	0.57	0.42	0.42	0.42	0.39	0.42
Mg	2.63	2.71	2.42	2.35	2.33	2.35	3.16	3.1	3.29
Ti	-	-	-	0.01	0.01	0.01	0.13	0.12	0.37
Cr	-	-	0.01	-	0.04	0.04	0.01	0.01	0.09
Mn	-	-	0.01	0.01	-	-	-	-	0.01
Co	-	-	0.01	0.01	-	0.01	-	-	-
Ni	0.04	0.04	0.09	0.08	0.13	0.13	0.96	0.96	0.08
Sum_{Oct}	3.02	3.06	3.05	3.03	3	3.01	5.73	5.71	5.27
Na	-	-	-	-	-	-	-	0.01	0.01
K	-	-	-	-	0.01	-	-	-	-
Ca	0.01	-	-	0.01	0.02	0.01	-	-	-
Sum_{Int}	0.01	-	-	0.01	0.03	0.01	-	0.01	0.02

Notes: - = not detected; a.p.f.u. = atoms per formula unit

by Mn oxyhydroxide encrustations, while spinels grains are enclosed in a Fe oxyhydroxide-rich matrix. As expected, Fe is distributed in Fe oxyhydroxides and spinels (Fig. 12B). Manganese and Cr are mostly concentrated in Mn oxyhydroxides (Fig. 12C) and spinels (Fig. 12D), respectively. Moreover, lower Mn amounts were also detected in spinel grains. Interestingly, Mn oxyhydroxides exert a strong control on the Ni distribution (Fig. 12E). Conversely, Co is found to be equally distributed among Fe and Mn oxyhydroxides and is highly concentrated in spinels grains (Fig. 12F).

Discussion

Genesis and evolution of the Santa Fé deposit: From an alkaline ultramafic intrusion to an oxide-dominated laterite

The mineral paragenesis of the Santa Fé laterite is shown in Figure 13. Ferromagnesian minerals (olivine and pyroxene), apatite and primary Fe-Cr (chromite, ferritchromite I and II, magnetite I, and hematite I), and Ti oxides (perovskite, ilmenite, and Ti/Al oxide I) represent the earliest formed minerals. Olivine and pyroxene represent remnants of parent rocks preserved in the saprock horizon, while Fe-Cr oxides, as well as apatite and Ti/Al oxides occur also in the upper zones of the profile. Although ilmenite and Ti/Al oxide are found as exsolution lamellae in magnetite I and perovskite, respectively, their formation from alkaline melts is gener-

ally related to very different stages of the evolution of the orthomagmatic system. Such trellis-type ilmenite exsolution commonly indicates an oxyexsolution process occurring at magmatic temperatures (T > 600°C; Tan et al., 2016), while Ti/Al oxide-rich exsolution in perovskite mainly forms at lower temperatures (T < 350°C; Chakhmouradian and Mitchell, 2000), typical of later hydrothermal alteration stages. The olivine and pyroxene replacement by serpentine I is also related to a hydrothermal alteration stage that occurred prior to lateritization. Mineralogical characteristics of serpentinites are related to both the original mineralogy of the protolith and to the hydrothermal fluid oxidation state (e.g., Mével, 2003; Lambiv Dzemua and Gleeson, 2012; Evans et al., 2013, and references therein). Hydrothermal alteration of olivine-pyroxene–dominated cumulates produces a serpentine-brucite-magnetite assemblage (e.g., Mével, 2003), whereas high silica activity allows formation of cryptocrystalline quartz, as observed at Santa Fé.

Ferritchromite is one of the main minerals in the saprock and green saprolite, widespread in the oxyhydroxide section of the weathering profile. Ferritchromite did not form directly from the crystallization of the magma, but as an alteration product of Al spinel and chromite (e.g., Merlini et al., 2009; Lambiv Dzemua and Gleeson, 2012). Mellini et al. (2005) showed that chromite alteration to ferritchromite and/or Cr magnetite is common during late stages of regional ser-

Table 6. Chemical Composition (wt %) of Selected Mn Oxyhydroxides

Oxides	Romanèchite		Asbolane		Lithiophorite	
Na_2O	-	0.03	-	-	0.17	0.23
MgO	3.61	1.53	0.98	1.53	19.79	17.3
Al_2O_3	0.36	0.49	0.62	0.45	19.79	17.3
SiO_2	4.6	2.55	0.89	1.06	0.43	1.11
K_2O	0.01	0.05	-	-	-	-
CaO	0.07	0.18	-	-	-	-
TiO_2	0.23	0.13	0.18	0.23	0.12	0.1
Cr_2O_3	0.04	-	-	-	0.03	-
MnO	37.74	41.86	42.56	46.7	39.17	40.43
FeO_t	4.76	3.16	8.64	6.17	9.64	6.21
CoO	3.71	3.55	2	2.52	2.8	3.56
NiO	12.52	13.79	20.13	19.39	6.87	9.46
BaO	5.29	4.97	-	-	-	0.32
Total	72.88	72.27	76.01	78.06	79.02	78.72
	a.p.f.u. on the basis of O_{10}		a.p.f.u. on the basis of $O_2(OH)_2$		a.p.f.u. on the basis of $O_2(OH)_2$	
Na	-	0.01	-	-	-	-
Mg	0.6	0.26	0.05	0.07	0.01	0.01
Al	0.05	0.07	0.02	0.02	0.64	0.57
Si	0.51	0.29	0.03	0.03	0.01	0.03
K	0	0.01	-	-	-	-
Ca	0.01	0.02	-	-	-	-
Ti	0.02	0.01	-	0.01	-	-
Cr	-	-	-	-	-	-
Mn	2.92	3.32	0.96	1.02	0.74	0.78
Fe	0.4	0.27	0.21	0.15	0.2	0.13
Co	0.3	0.3	0.05	0.06	0.06	0.07
Ni	1.13	1.28	0.53	0.49	0.15	0.21
Ba	0.23	0.22	-	-	-	-

Notes: - = not detected; a.p.f.u. = atoms per formula unit

Table 7. Chemical Composition (wt %) of Selected Fe Oxyhydroxides

Oxide	Hematite				Goethite			
Na_2O	0.15	-	0.31	0.19	0.07	-	-	-
MgO	1.53	0.38	0.02	0.13	0.02	0.27	-	-
Al_2O_3	0.09	2.78	2.57	2.95	5.57	5.42	4.69	3.4
SiO_2	1.3	2.46	2.8	2.59	2.74	1.58	2.91	2.05
K_2O	-	-	-	-	0.04	-	0.01	0.02
CaO	0.06	0.07	0.07	0.06	-	-	-	-
TiO_2	0.12	0.38	0.3	0.58	0.32	0.68	1.52	0.83
Cr_2O_3	0.13	0.45	0.77	0.67	1.89	0.66	0.66	1.8
MnO	1.59	0.43	0.14	0.34	0.14	0.26	0.59	0.14
FeO_t	94.82	91.1	90.52	89.69	78.08	79.02	78.68	80.71
CoO	0.36	0.43	0.37	0.34	0.36	0.37	0.39	0.19
NiO	0.22	0.55	0.61	0.85	0.74	1.63	0.41	0.59
Total	100.36	99.03	98.48	98.39	89.95	89.89	89.86	89.84

Notes: - = not detected

pentinization of spinel-bearing dunites, accompanied by chlorite precipitation. Moreover, Colás et al. (2017) showed that SiO_2-rich hydrothermal fluids during low-temperature serpentinization of ferromagnesian minerals enhance the metamorphism of primary chromite, leading to a Fe^{3+}-rich spinel + chlorite assemblage. At Santa Fé this process is visible in the early paragenetic evolution of chromite to ferritchromite I. Late chromite alteration to ferritchromite supplied high amounts of Cr, Mg, and Al to the system (Fig. 10D), which in the presence of high-SiO_2, triggered chlorite formation. This explains the close paragenetic association observed between chlorite-ferritchromite (Fig. 7F) and chlorite with cryptocrystalline quartz (Fig. 7E). High Cr and low Mg numbers of ferritchromite (Fig. 10C) and the occurrence of ferropargasite inclusions in spinels (Fig. 8H) indicate a high-temperature alteration process, under retrograde amphibolite facies metamorphism (Barnes and Roeder, 2001; Mellini et al., 2005; Arai et al., 2006; Arai and Akizawa, 2014).

Early supergene processes were likely related to the Sul-Americano weathering cycle (Eocene to Oligocene; Braun, 1970), largely recorded by silcrete layers. Silica-rich sections within the weathering profiles have been reported in many Ni laterite deposits, as in Australia (e.g., Mt. Keith and Wingellina, Butt and Nickel, 1981; Putzolu et al., 2018, 2019), in
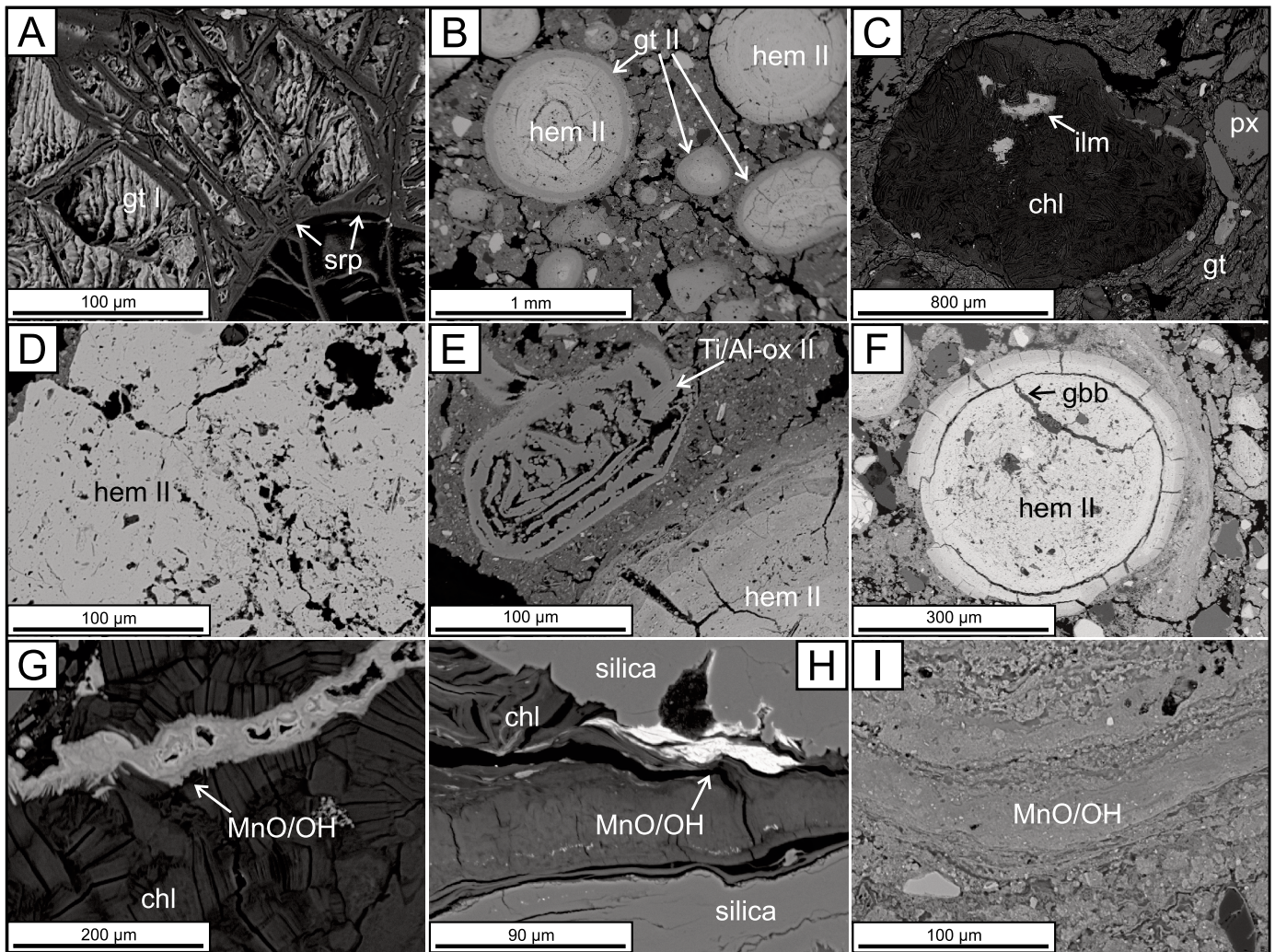
Fig. 9. Backscattered electron photomicrographs showing the typical textures of supergene oxyhydroxides. A) Skeletal goethite enveloped in serpentine mesh (saprock). B) Oolitic Fe oxyhydroxides (ferruginous saprolite). C) Detrital chlorite and pyroxene in a goethite-rich matrix (ferruginous saprolite). D) Massive hematite crust (lateritic crust). E) Neoformed Ti/Al oxide (Ti/Al-ox II) in goethite matrix (ferruginous saprolite). F) Gibbsite crosscutting hematite (lateritic crust). G) Mn hydroxide vein crosscutting chlorite (saprock). H) Mn oxyhydroxide replacing chlorite (saprock). I) Layered Mn oxyhydroxide encrustation (lateritic crust). Mineral abbreviations: chl = chlorite, gbb = gibbsite, gt = goethite, hem = hematite, ilm = ilmenite, MnO/OH = Mn oxyhydroxide, px = pyroxene, srp = serpentine, Ti/Al-ox = Ti/Al oxide.

the Mediterranean area (e.g., Çaldağ, Thorne et al., 2009), and in Brazil (de Oliveira et al., 1992), and are a common feature of laterites derived from olivine-dominated cumulates (i.e., dunite; Butt and Cluzel, 2013, and references therein). Silica precipitation occurs by evapotranspirative oversaturation of silicic acid formed either during the olivine hydrolysis or due to serpentine decomposition (e.g., Thorne et al., 2009). However, it is widely accepted that silicification is an alteration process mainly developed during arid to semiarid climatic stages, rather than during tropical weathering sensu stricto (e.g., Golightly, 2010, and references therein).

Lateritic weathering sensu stricto likely started with the onset of the Velhas cycle (Braun, 1971). Evidence for this includes formation of Ni-rich serpentine (srp II), skeletal goethite (ght I), smectite clays, and Mn oxyhydroxides. Serpentine II was developed directly from serpentine I, whereas both goethite I and smectite formed from olivine. Neverthe-

less, as shown by Golightly (2010, and references therein), genesis of smectite at Santa Fé was controlled by alteration of pyroxene. Given that minor smectite and Mn hydroxides are found in the lowermost section of the profile (i.e., saprock), while in situ goethite I occurs in the green saprolite unit in the mesh cores, less acidic conditions and a lower degree of leaching have enhanced the stability of clays and of Mn oxyhydroxides deeper in the profile (Velde and Meunier, 2008; Golightly, 2010; Dublet et al., 2017). In contrast, in the uppermost zones, two distinct processes could have developed: either olivine weathered directly to skeletal goethite or smectite decomposed to Fe oxyhydroxides following the typical paragenetic sequence observed in many laterite profiles worldwide (e.g., Freyssinet et al., 2005, and references therein; Tauler et al., 2017; Putzolu et al., 2019; Teitler et al., 2019). The occurrence of newly formed Ti phases (i.e., Ti/Al-Fe oxides) and gibbsite cements in the uppermost sec-
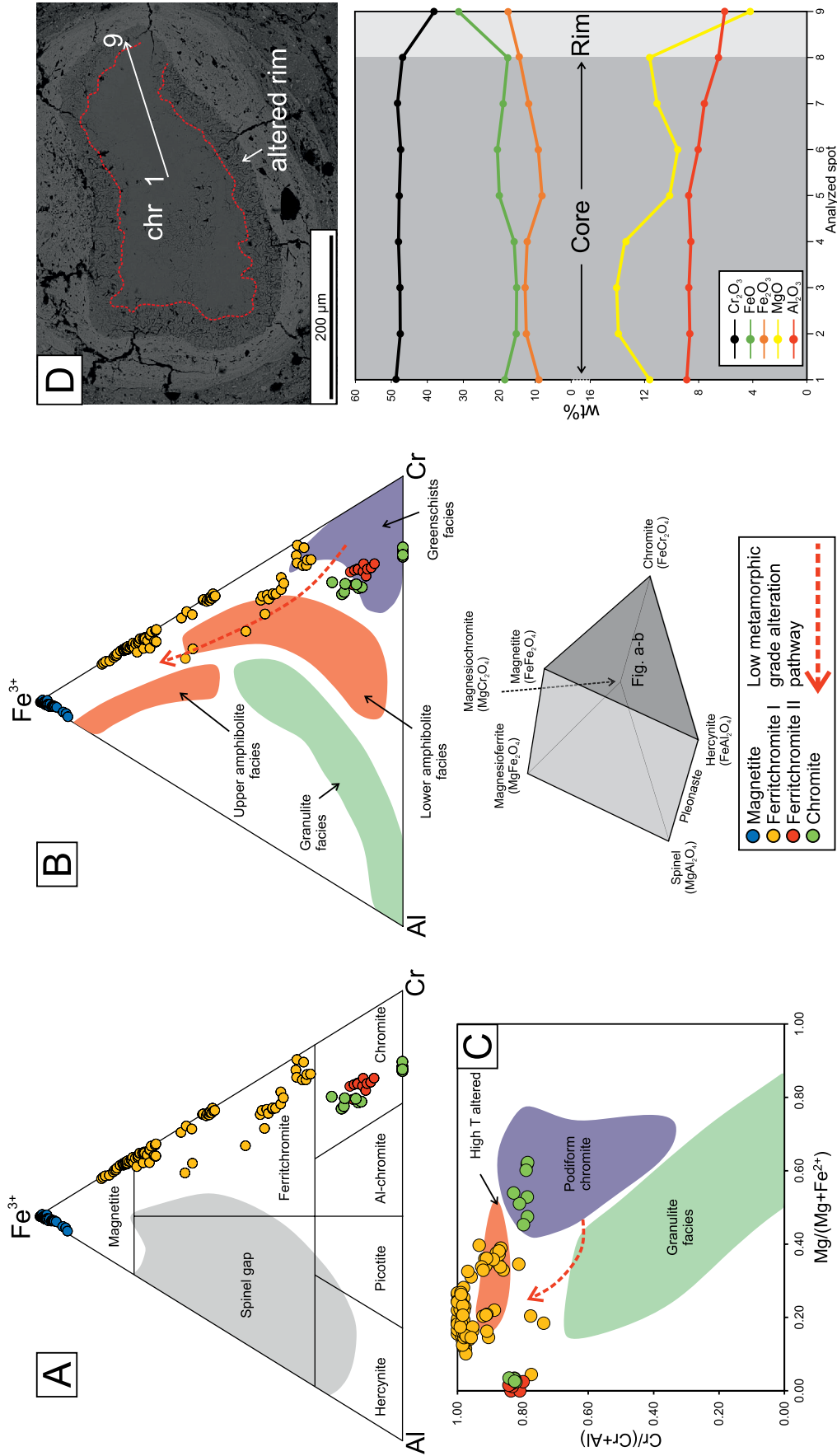
Fig. 10. A, B) Ternary plots showing the mineralogy and chemistry of spinels, respectively. C) Mg# versus Cr# binary plot showing the chemical variation between chromite (chr) and ferritchromite (I and II) (adapted from Akizawa and Arai, 2009). D) Geochemical transect in an altered chromite grain. Compositional and metamorphic fields of A and B are from Barnes and Roeder (2001) and Evans and Frost (1976), respectively.
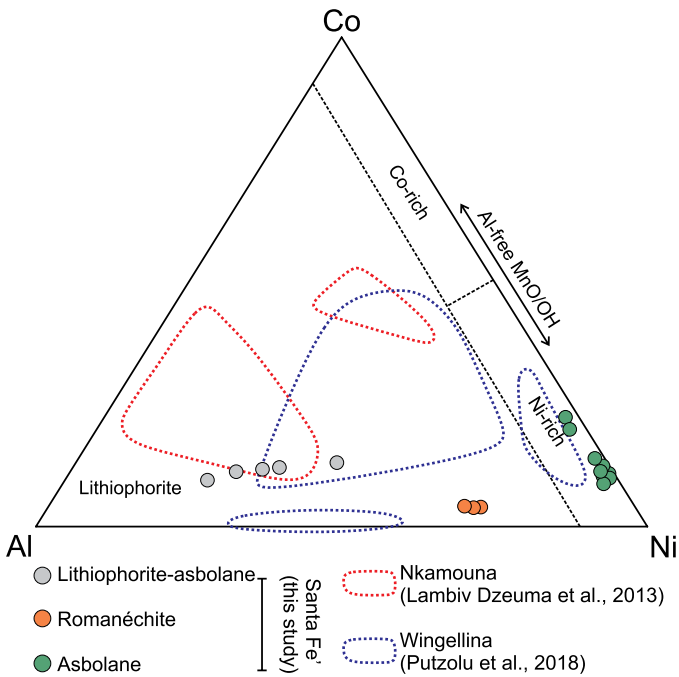
Fig. 11. Co-Ni-Al ternary plot (cationic composition wt %) displaying the mineral chemistry of Mn oxyhydroxides from Santa Fé and comparing their composition to those from Wingellina, Western Australia (Putzolu et al., 2018) and Nkamouna, southeast Cameroon (Lambiv Dzemua et al., 2013).

tion of the deposit indicates that during the ferrugination stage, Ti and Al were liberated from earlier mineral phases (i.e., Ti from Ti/Al oxide I and Al from chlorite, lithiophorite-asbolane, and chromite) and concentrated in late-stage oxyhydroxides. The occurrence of oolitic Fe oxyhydroxides and of detrital goethite I and chlorite from the ferruginous saprolite likely records a partial reworking and collapse of the ferruginous zones, which, together with further coeval lateritization, obliterated the original textures.

Element distribution and Ni-Co deportment

In accordance with the model of direct formation of Ni laterites (e.g., Golightly, 2010), in which groundwater flushing enhances leaching of Mg and Si following the decomposition of ferromagnesian minerals, we also see almost complete leaching of Mg and Si at Santa Fé. This process normally produces an oxide-dominated regolith, where Ni and other transition metals are enriched into Fe oxyhydroxides (e.g., Freyssinet et al., 2005; Elias, 2006; Butt and Cluzel, 2013). However, at Santa Fé, most of the variance of Ni is not correlated with Fe (Fig. 5A, B). To decipher the Ni distribution in the Santa Fé deposit, it has to be considered that PC1 explains the behavior of elements whose pathways are totally controlled by the lateritization-related leaching (i.e., Mg and Si) or precipitation in neoformed phases (i.e., Fe). In this context, the geochemical decoupling of the Ti-Al-P-Ca and Mn-Co-Cr-Ni groups from the anticorrelated Mg-Si versus Fe group (Fig. 5B) can be explained by some key elements being hosted in weathering-resistant phases. In detail, the Ti-Al-P-Ca group is indicative of the occurrence of preweathering primary Ti oxides (Ti/Al oxide I, ilmenite, and perovskite) as well as apatite throughout the weathering profile. The Mn-Co-Cr-Ni group

also includes Cr, suggesting that part of the variance might be controlled by the element distribution in the magmatic to hydrothermal Cr-Fe oxides, widely identified in oxide-dominated zones of the deposit. Therefore, the occurrence of the Ni eigenvector in that group indicates that Ni distribution is not explained only by the distribution of newly formed Ni-bearing Fe oxyhydroxides. At Santa Fé the highest Ni grades occur in chlorite minerals (up to 11 wt % NiO), which are not only are the main constituents of the phyllosilicate-rich zones of the orebody but are also enriched as detrital minerals in the uppermost section of the regolith profile. Although the formation of chlorite at Santa Fé cannot be directly ascribed to the lateritization stage sensu stricto, many studies (e.g., Wiewiòra and Szpila, 1975; Noack and Colin, 1986; Suarez et al., 2011) have highlighted that chlorite can act as scavenger for Ni. The importance of chlorite distribution in the Fe oxyhydroxide-rich units of the orebody can be also deciphered by the MgO-SiO_2-(Al_2O_3 + Fe_2O_3) ternary plot (Fig. 3), where a significant increase of the UMIA can be followed from the R6 unit up core. In spite of this, many analyses from the transition zone and the lateritic crust fall outside the compositional field of typical oxide-dominated lithologies observed in the in situ deposits (e.g., Aiglsperger et al., 2016; Tauler et al., 2017; Putzolu et al., 2019) and are shifted toward the MgO-rich field of the plot. Therefore, the complex Ni distribution in the Santa Fé deposit and the noncorrelation between Ni and Fe observed in the full data set PCA (Fig. 5A) are related to the in situ coeval ferrugination, which accounted for both a partial Ni scavenging by Fe oxyhydroxides and partial reworking, producing an exotic input of Ni-rich chlorite.

The Co speciation in laterite profiles is commonly controlled by the distribution of Mn oxyhydroxides because of their high capability incorporate trace elements (Burns, 1976; McKenzie, 1989; Manceau et al., 1992; Kay et al., 2001; Lambiv Dzemua and Gleeson, 2012; Aiglsperger et al., 2016; Putzolu et al., 2018, 2019). The enrichment process during lateritization is controlled by the availability of Co and Mn in the magmatic bedrock and by the reaction pathways during the regolith evolution. In most ultramafic-derived laterites, Co and Mn (as well as Ni) are sourced from olivine (e.g., Dublet et al., 2017). Under neutral pH to slightly alkaline conditions, commonly detected in the deeper parts of the laterite profile, the oxidation of Co to the trivalent state (Co^{3+}) and of Mn to the tetravalent state (Mn^{4+}) would cause the formation of Co-bearing Mn oxyhydroxides (Burns, 1976; Dublet et al., 2017) and eventually the economic concentration of Co. At Santa Fé, the presence of Co-bearing Mn oxyhydroxides is limited, and their Co grade is generally lower compared with other oxide-dominated laterite deposits (Fig. 11). Moreover, the variation of Co in the whole data set (Fig. 5A, B) suggests that the Co deportment is not entirely controlled by Mn oxyhydroxides. Moreover, initial Mn and Co contents of the Santa Fé ultramafic rocks (mean = 0.01 wt % Co and 0.17 wt % MnO) are comparable with protoliths of other Ni- and Co-fertile laterites, like Wingellina (Western Australia, Putzolu et al., 2019). However, the Santa Fé weathered profiles are relatively depleted in Co and Mn (mean = 0.08 wt % CoO and 0.75 wt % MnO), compared to other Ni- and Co-fertile laterites. The most important reasons for the lack of enrichment in Co in the Santa Fé later-

ites, as well as for its peculiar association not only with Mn but also with Cr, are linked to the petrological characteristics of the parent rock and to its hydrothermal alteration history. Here, fresh bedrock represents the mafic to ultramafic plutonic component of a large magmatic province with alkaline affinity (e.g., Barbour et al., 1979; Brod et al., 2005). The behavior of Co in subalkaline basaltic melts, such as in the parent rocks of the Ni-Co Wingellina deposit in Western Australia (Ballhaus and Glikson, 1995), favors its incorporation in olivine (partition coefficient [Kd] up to 6.5; Mysen, 2007) and less in clinopyroxene (Kd = 1.32; Bougault and Hekinian, 1974). In basaltic melts with alkaline affinity, Co has instead a higher affinity with spinels (Kd = 4.7–8.3; Horn et al., 1994) than with ferromagnesian minerals (i.e., olivine Kd = 5.1, clinopyroxene Kd = 1.02; Villemant et al., 1981). In the case of Santa Fé, this process would explain the relative high Co content detected in primary Cr spinels (up to 0.53 wt % CoO in chromite), and the corresponding low Co concentration in olivine (up to 0.08 wt % CoO). Moreover, another factor that has enhanced the trace element gain in Cr-Fe spinels is the hydrothermal alteration of chromite, leading to formation of ferritchromite I and II. At Santa Fé,

the significant redistribution of transition metals during the hydrothermal alteration of magmatic spinels is shown by elevated Mn, Ni, Co, and Zn in late-stage spinels, and by the presence of Ni- and Co-bearing Fe-sulfide inclusions within the spinels themselves (Fig. 8E). Moreover, the postmagmatic alteration of spinels at Santa Fé is also corroborated by their Mg and Cr numbers, highlighting a hydrothermally related depletion of Al and Mg compared to nominal magmatic chromite (Barnes and Roeder, 2001). Postmagmatic alteration of Cr spinel plays a primary role also in defining the trace element (mostly Mn, Zn, Co, Ni) budget in late-stage spinels (e.g., Economou-Eliopoulos, 2003; Ożóg and Pieczonka, 2019). At the scale of the whole deposit, the Co (and Mn) affinity to spinels has been observed through PCA (Fig. 5B-E), where most of the Co variance is correlated to Cr and Mn (Fig. 5B, C), while a clear geochemical and thus mineralogical Co differentiation to spinels is visible only in minor components (i.e., PC4 and PC5), highlighting that part of Co has been scavenged to Fe and Mn oxyhydroxides (Fig. 5D, E).

The Co pathway during the prelateritic and early supergene stages in the Santa Fé deposit is summarized in a three-stage
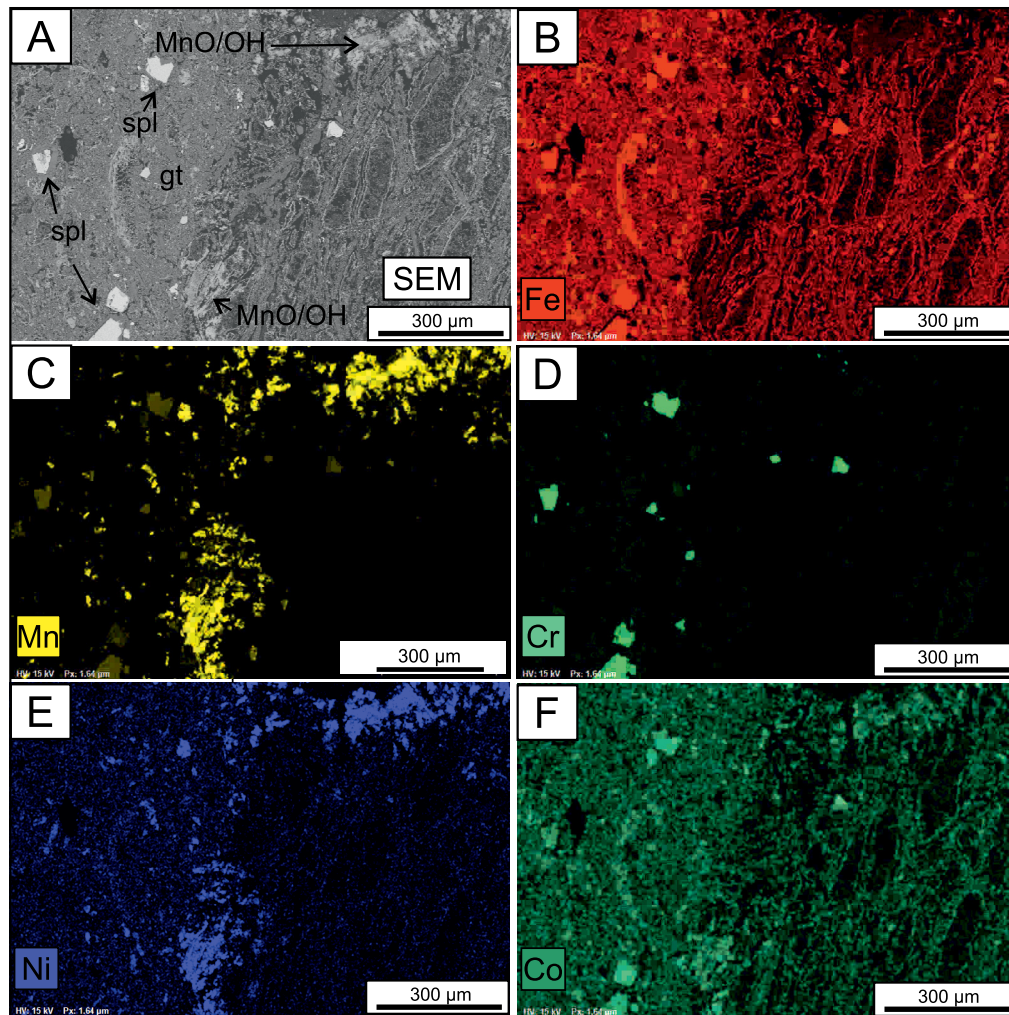

Fig. 12. (A-F) EDX high-resolution maps of Fe and Mn oxyhydroxide region in the ferruginous saprolite (R6). Abbreviations: gt = goethite, spl = spinel.
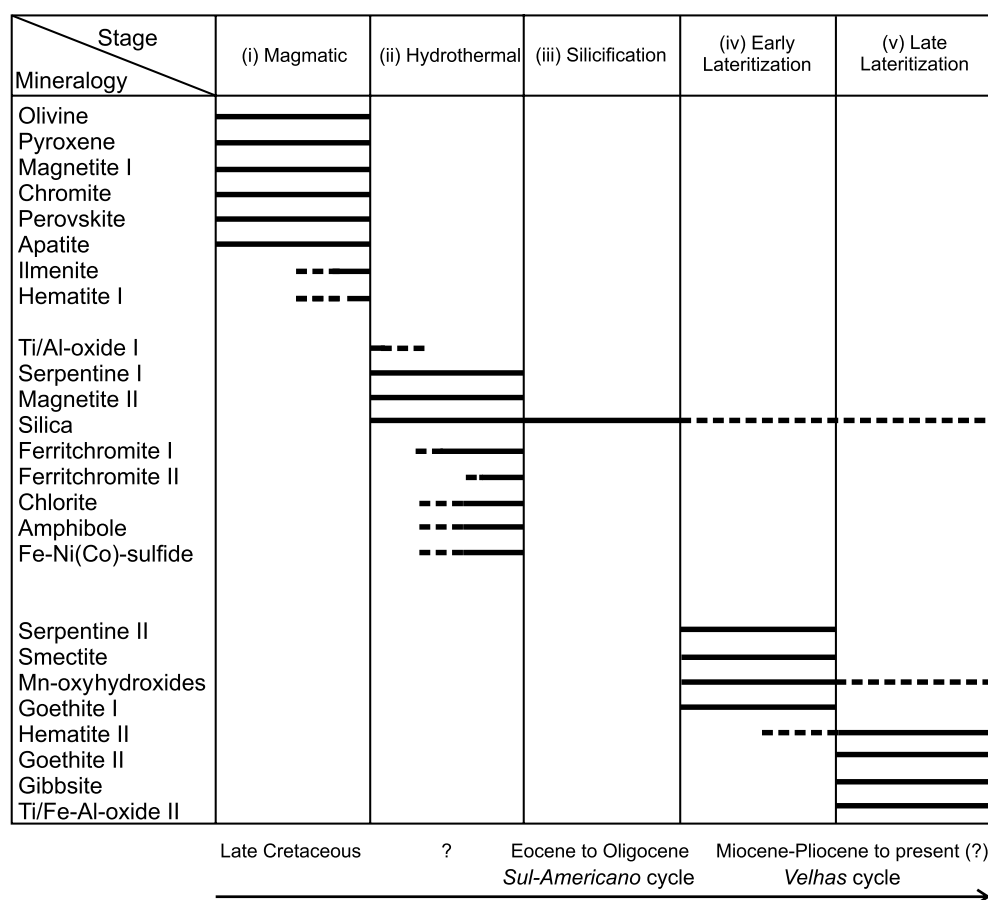
Stage / Mineralogy	(i) Magmatic	(ii) Hydrothermal	(iii) Silicification	(iv) Early Lateritization	(v) Late Lateritization
Olivine	▬				
Pyroxene	▬				
Magnetite I	▬				
Chromite	▬				
Perovskite	▬				
Apatite	▬				
Ilmenite	▬ ▬				
Hematite I	▬ ▬				
Ti/Al-oxide I		▬ ▬			
Serpentine I		▬			
Magnetite II		▬			
Silica		▬	▬	- - - - -	- - - - -
Ferritchromite I		▪ ▬			
Ferritchromite II		▬			
Chlorite		▪ ▪ ▬			
Amphibole		▪ ▪ ▬			
Fe-Ni(Co)-sulfide		▪ ▪ ▬			
Serpentine II				▬	
Smectite				▬	
Mn-oxyhydroxides				▬	- - - -
Goethite I				▬	
Hematite II					- - - ▬
Goethite II					▬
Gibbsite					▬
Ti/Fe-Al-oxide II					▬
	Late Cretaceous	?	Eocene to Oligocene *Sul-Americano* cycle	Miocene-Pliocene to present (?) *Velhas* cycle	

Fig. 13. Mineral paragenesis in the Santa Fé laterite deposit.

model (Fig. 14). This model shows that primary Cr spinels (i.e., chromite) contain Co and Mn because of their relatively high partitioning during the orthomagmatic stage (Fig. 14A). During the early alteration stage, the hydrothermal process was only effective in triggering the olivine-to-serpentine transformation (i.e., serpentinization), which led to the leaching of Mg, Si, Ni, and Co^{2+} hosted in olivine. In this context, primary Cr spinels (i.e., chromite) remained unaltered, likely because of the highly reducing conditions occurring during serpentinization (Bach et al., 2006). However, while the SiO_2 and O_2 activity of the hydrothermal fluids increased, chromite lost Al^{3+} and Mg while Fe^{2+} in the Cr spinels oxidized to Fe^{3+} (Gonzáles-Jimenez et al., 2009). These processes, occurring during the retrograde metamorphic amphibolite stage, led to the formation of the Fe^{3+}-bearing ferritchromite rims, the chlorite alteration patches on spinels and the ferro-pargasite inclusions (Fig. 14B). A big part of Ni released by dissolution of olivine was taken up by chlorite, with less concentrated in late-stage spinels (i.e., ferritchromite I and II). On the contrary, the bulk of available Co was concentrated in spinels, the only phases able to do so at this time. When early supergene processes were superimposed on prelateritic processes (Fig. 14C), goethite I pseudomorphs formed from relict olivine and Mn oxyhydroxides replaced Ni chlorite and Fe oxyhydroxide rims formed upon spinels. In this scenario, the close paragenetic association between chlorite and Mn oxyhydroxides is clear evidence of the Ni uptake in lithiophorite-asbolane and

in other Mn species. However, as most of the Co was concentrated in late-stage spinels, little Co was available for redistribution and enrichment in supergene Mn oxyhydroxides, leading to the low Co concentrations displayed by these phases at Santa Fé (Figs. 11, 12).

The characteristics of the Santa Fé bedrock are also a likely strong control to the paucity of Mn oxyhydroxides in the laterite profile. Many studies (e.g., Taylor et al., 1964; McKenzie, 1989; Dowding and Fey, 2007; Roqué-Rosell et al., 2010; Lambiv Dzemua et al., 2013; Putzolu et al., 2018) have highlighted the primary role of late-stage lithiophorite and/or lithiophorite-asbolane intermediates in improving the stability of Mn oxyhydroxides. The formation of significant amounts of lithiophorite occurs if sufficient Al is available in the system (Cui et al., 2009). In the specific case of laterites, lithiophorite formation is restricted to those deposits derived from a magmatic intrusion containing Al-rich phases (e.g., plagioclase; Putzolu et al, 2018). Low levels of such minerals at Santa Fé in the protolith would have limited the formation of stable Mn oxyhydroxides. In fact, the majority of the lithiophorite-asbolane is associated with chlorite, the only phase containing significant Al.

The residual enrichment of Mn and Ni in late-stage goethite reflects the dissolution of preexisting Mn-Ni phases, such as more unstable Mn oxyhydroxides (e.g., asbolane and romanèchite). A similar partitioning of Mn has been observed by Dublet et al. (2015, 2017) in the New Caledonia laterites, with the notable exception that here, the dissolution of Mn

oxyhydroxides do not lead to a significant Co enrichment in the latest goethite formed.

Implications for ore processing and metal recovery

The Santa Fé lateritic ore, characterized by a dominant oxide-rich zone (goethite and hematite), is different from other major laterite deposits of the Goiás State, such as Niquelândia and Barro Alto (de Oliveira et al., 1992). In both of these deposits, the exploitation is focused on Ni, recovered from the saprolitic layers enriched in Mg(Ni) phyllosilicates (e.g., Colin
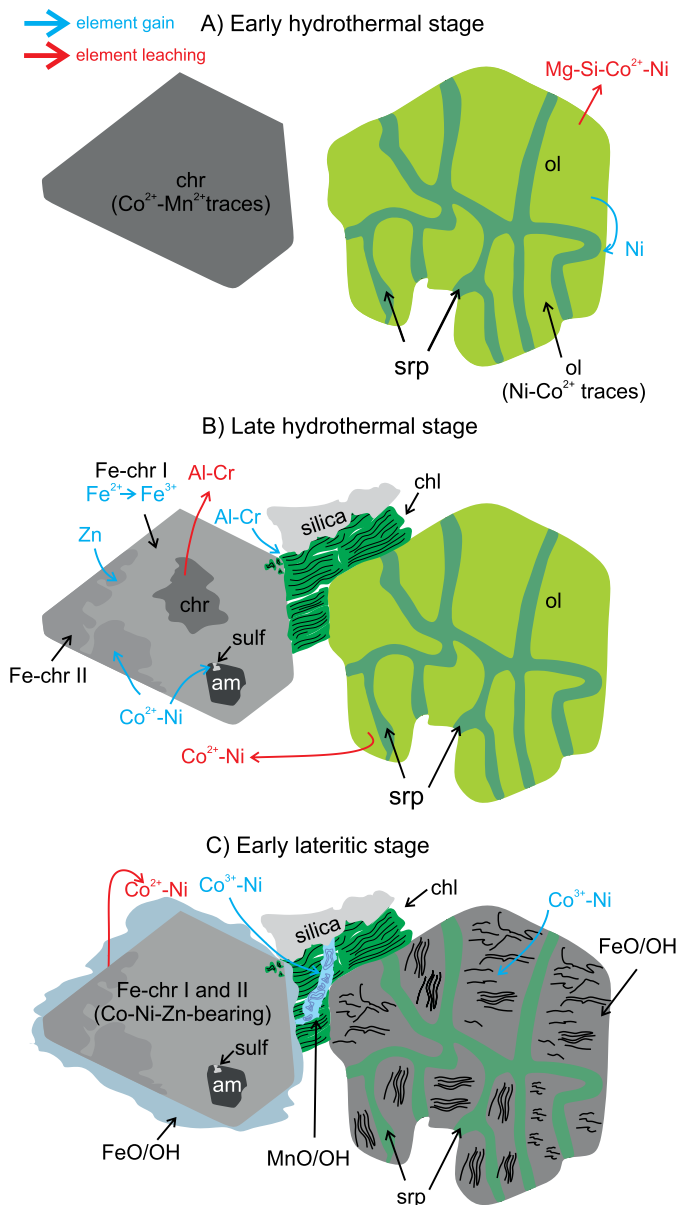

Fig. 14. Schematic sketch illustrating the mineralogical and compositional changes in prelateritic and synlateritic phases at Santa Fé. Emphasis is given to the relationship between the element pathways and the paragenetic evolution of the mineralogical assemblage. Minerals abbreviations: am = amphibole, chl = chlorite, chr = chromite, Fe-chr = ferritchromite, FeO/OH = Fe oxyhydroxide, MnO/OH = Mn oxyhydroxide, ol = olivine, srp = serpentine, sulf = sulfide. Notes: A and B correspond to the incipient and late phases, respectively, of the (ii) stage in the paragenetic sketch; C corresponds to the (iv) phase in the paragenetic sketch.

et al., 1990; Ratié et al., 2015). In the Niquelândia deposit the main ore mineral is Ni smectite, while at Barro Alto the main orebody is composed of Ni serpentine and garnierite (Ratié et al., 2015). The chemistry of the saprolite ore in these deposits, also characterized by negligible Fe contents and by low SiO_2/MgO ratios, is ideal for pyrometallurgical ore processing (i.e., smelting), to produce ferronickel alloys with a favorable Fe/Ni ratio (Crundwell et al., 2011; Ratié et al., 2016, and references therein). In the specific case of Santa Fé, the most significant characteristics to take into account while planning the processing method are (1) oxide-bearing units dominate compared to phyllosilicate-rich layers, (2) the highest Ni grades occur within the ferruginous saprolite, associated with goethite and chlorite, and (3) the cobalt deportment in the laterite profile is controlled by both newly formed oxyhydroxides and spinels. A key observation is the strong affinity of Co to spinel phases. Metallurgical processes most widely adopted for Ni laterites are not effective at dissolving spinels, leaving behind a residuum consisting either of silicate slag produced by pyrometallurgical methods or of quartz, spinels, and other minerals and/or alloys if leaching methods as high-pressure acid leaching (HPAL; Valix and Cheung, 2002; Dalvi et al., 2004, and references therein). The proportions of Co locked in spinels versus Co concentrated in late-stage minerals can be assessed by looking at the results of preliminary metallurgical tests undertaken on the Santa Fé oxide ore (Dreisinger et al., 2008). Metal recoveries were tested through HPAL, by using H_2SO_4 (at 250°C for 60 min) as leaching agent and saprolite lithologies (R7 unit) as acid neutralization agent. The feeds consisted of several blends of the R3, R5, and R6 units (Table 8). Prior to the leaching test, and in order to upgrade the Ni content of the feed, test material was subjected to a mineral beneficiation step using magnetic and heavy mineral separation, likely resulting in the removal of the bulk of the Co-bearing spinels. By comparing the chemistry of the feeds after the mineral beneficiation step with the chemistry of the average Santa Fé ore (Fig. 15), it can be observed that the pretreatment of the ore was effective only in upgrading Ni and not Co. Increase in Mg can be explained by its occurrence in chlorite together with Ni. Cobalt and Cr were actually downgraded during beneficiation with respect to the chemistry of the R3, R5, and R6 ore zones (Fig. 15), thus confirming that Co-bearing spinels are removed during the beneficiation. The observed downgrade indicates that the portion of Co locked in spinels varies between 20 and 50% in the various ore zones (Table 8).

Conclusions and Implications

The Santa Fé laterite has a complex multistage history, starting with a postmagmatic hydrothermal alteration of the parent rock, followed by two main supergene alteration stages, involving an early-stage silicification followed by a lateritization sensu stricto.

The Santa Fé deposit can be classified as an oxide-type deposit, where goethite and hematite represent the most abundant Ni-containing minerals. The silicate-dominated sections of the orebody host also a Ni-rich chlorite and serpentine. Despite the above classification, the Ni pathway in the Santa Fé deposit is different from other oxide-dominated ores and thus cannot be only explained by its uptake by Fe oxyhydroxides. As shown by multivariate analyses, in situ ferrugination does

Table 8. Comparison Between the Chemistry of the Feeds for Metallurgical Test Works and the Assay Data

| Description | Reference | Metallurgical test data (wt %) | | | | | | | |
		Al	Co	Cr	Fe	Mg	Mn	Ni	Si
Pressure acid leach blend 1	Dreisinger et al. (2008)	1.50	0.06	2.05	34.30	6.30	0.63	1.59	10.30
Pressure acid leach blend 2		1.15	0.05	1.70	30.50	6.50	0.53	1.47	12.70
Pressure acid leach blend 3		1.73	0.04	1.06	30.20	6.20	0.52	1.49	12.70
Saprolite neutralization blend 1		1.71	0.02	0.83	14.50	15.00	0.28	1.66	16.60
Saprolite neutralization blend 2		0.40	0.02	0.71	17.70	13.80	0.31	1.76	16.10

| Description | Reference | Whole-rock chemical data (wt %) | | | | | | | |
		Al	Co	Cr	Fe	Mg	Mn	Ni	Si
R3 unit avg chemistry (assay)	This study	2.12	0.10	2.89	38.40	1.88	0.66	0.91	10.59
R5 unit avg chemistry (assay)		1.46	0.09	2.11	39.29	2.42	0.72	1.43	9.82
R6 unit avg chemistry (assay)		2.27	0.06	1.44	30.22	4.67	0.53	1.37	13.11
Average chemistry R3+R5+R6 (assay)		1.95	0.09	2.15	35.97	2.99	0.64	1.24	11.17
Santa Fé bulk chemistry (assay)		1.85	0.08	2.03	30.73	5.87	0.58	0.84	12.70

| Description | Reference | Concentration ratios | | | | | | | |
		Al	Co	Cr	Fe	Mg	Mn	Ni	Si
Avg chemistry of blends/R3 avg assay	This study	0.69	0.50	0.55	0.82	3.37	0.85	1.67	1.12
Avg chemistry of blends/R5 avg assay		1.00	0.55	0.76	0.81	2.61	0.78	1.06	1.21
Avg chemistry of blends/R3 + R5 + R6 avg assay		0.64	0.80	1.11	1.05	1.36	1.05	1.11	0.91
Avg chemistry of blends/R6 avg assay		0.75	0.59	0.75	0.88	2.12	0.88	1.23	1.07
Avg chemistry of blends/Santa Fé bulk chemistry		0.79	0.64	0.79	1.03	1.08	0.96	1.81	0.94

not account for the statistical distribution of Ni throughout the laterite facies of the Santa Fé ore. The process accounting for the geochemical decoupling between the Fe_2O_3- and Ni-rich facies of the deposit is the extensive erosion of the regolith during the lateritization stage, which resulted in the reworking of Ni-bearing chlorite in the ferruginous units of the ore that has obscured the in situ geochemical footprint of Ni.

The Santa Fé deposit is an atypical oxide-type laterite also in terms of the observed Co distribution and speciation. According to the multivariate analyses, most of the statistical distribu-

tion of Co is correlated with that of Cr, rather than following the typical association with Mn and thus with Mn oxyhydroxides. The Co-Cr association is mainly related to the relatively high Co content detected in magmatic and hydrothermal (i.e., chromite and ferritchromite, respectively), which are residual phases inherited from the parent rock and are ubiquitous throughout the laterite profile. The prelateritic processes accounting for the Co enrichment in spinels can be related to the formation of the parent rock during the orthomagmatic stage and to its later hydrothermal history. During the ortho-
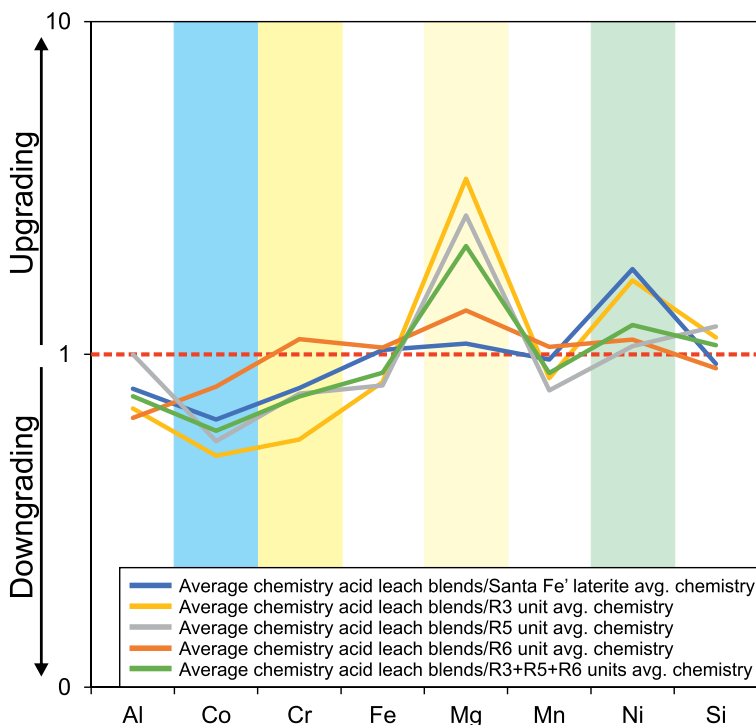

Fig. 15. Elemental ratios between the average composition of the screened feeds used for metallurgical test work and the various Santa Fé laterite ore facies. It can be seen that Ni and Mg are rich in the feed in respect to the ore, whereas Co and Cr are poor, suggesting that the Co-bearing phases have been removed during the screening. For tabulated data see Table 8.

magmatic stage, part of the Co was concentrated in chromite due to its high partitioning in Cr spinels forming from alkaline melts. The occurrence of the ferritchromite ± amphibole ± Fe-Ni(Co)-sulfide ± chlorite ± silica assemblage overprinting the magmatic mineralogical assemblage (i.e., olivine ± pyroxene ± Cr spinels) suggests that during the hydrothermal stage the Santa Fé ultramafic suite experienced amphibolite facies retrograde metamorphic conditions, which were able to trigger a mineralogical and chemical reset of primary spinels that enhanced the Co concentration in late-stage spinels. Both magmatic and hydrothermal processes ended with the Co concentration in phases that hardly experience significant dissolution during lateritization, thus limiting the Co availability during the supergene ore-formation stage and its secondary precipitation in the newly formed Mn and Fe oxyhydroxides.

Considering that during orthomagmatic processes the Co enrichment in primary Cr spinels might be significant in ultramafic alkaline systems, it is reasonable to suppose that laterites formed over alkaline intrusions are in general unlikely to become enriched in Co. However, as the Santa Fé case represents to date the first mentioned Ni laterite ore developed from an alkaline ultramafic body, this conclusion has to be verified conducting further studies on deposits originating from similar magmatic suites.

Since the Co enrichment in late-stage Fe spinels is closely related to the formation of ferritchromite and Al chlorite, these phases can be used as indicators to warn of potentially refractory Co in laterite systems. In the Santa Fé case, the interpretation of preliminary metallurgical test works suggests that spinels control a significant fraction of Co ranging between 20 and 50%.

Acknowledgments

REFERENCES

Aiglsperger, T., Proenza, J.A., Lewis, J.F., Labrador, M., Svojtka, M., Rojas-Purón, A., Longo, F., and Ďurišová, J., 2016, Critical metals (REE, Sc, PGE) in Ni laterites from Cuba and the Dominican Republic: Ore Geology Reviews, v. 73, p. 127–147.

Akizawa, N., and Arai, S., 2009, Petrologic profile of peridotite layers under a possible Moho in the northern Oman ophiolite: An example from Wadi Fizh: Journal of Mineralogical and Petrological Sciences, v. 104, p. 389–394.

Almeida, F.F.M., 1967, Origem e evolução da Plataforma Brasileira: Boletim da Divisão de Geologia e Mineralogia, v. 241, 36 p.

——1983, Relações tectônicas das rochas alcalinas mesozóicas da região meridional da Plataforma Sul-Americana: Revista Brasileira de Geociências, v. 13, p. 139–158.

Arai, S., and Akizawa, N., 2014, Precipitation and dissolution of chromite by hydrothermal solutions in the Oman ophiolite: New behavior of Cr and chromite: American Mineralogist, v. 99, p. 28–34.

Arai, S., Shimizu, Y., Ismail, S.A., and Ahmed, A.H., 2006, Low-T formation of high-Cr spinel with apparently primary chemical characteristics within podiform chromitite from Rayat, northeastern Iraq: Mineralogical Magazine, v. 70, p. 499–508.

Babechuk, M.G., Widdowson, M., and Kamber, B.S., 2014, Quantifying chemical weathering intensity and trace element release from two contrasting basalt profiles, Deccan Traps, India: Chemical Geology, v. 363, p. 56–75.

Bach, W., Paulick, H., Garrido, C.J., Ildefonse, B., Meurer, W.P., and Humphris, S.E., 2006, Unraveling the sequence of serpentinization reactions: Petrography, mineral chemistry, and petrophysics of serpentinites from MAR 15 N (ODP Leg 209, Site 1274): Geophysical Research Letters, v. 33, 3921443676.

Ballhaus, C., and Glikson, A.Y., 1995, The petrology of layered mafic-ultramafic intrusions of the Giles Complex, western Musgrave block, Western Australia: AGSO Journal of Australian Geology and Geophysics, v. 16, p. 69–90.

Barbour, A.P., Girardi, V.A., Kawashita, K., and de Souza, A.M.S., 1979, Geocronologia do complexo máfico-ultramáfico alcalino de Santa Fé, Goiás: Boletim IG, v. 10, p. 11–18.

Barnes, S.J., and Roeder, P.L., 2001, The range of spinel compositions in terrestrial mafic and ultramafic rocks: Journal of Petrology, v. 42, p. 2279–2302.

Bougault, H., and Hekinian, R., 1974, Rift valley in the Atlantic Ocean near 36 degrees 50'N; petrology and geochemistry of basalt rocks: Earth and Planetary Science Letters, v. 24, p. 249–261.

Braun, O.P., 1971, Contribuição à geomorfologia do Brasil Central: Revista Brasileira de Geografia, v. 32, p. 3–39.

Brod, J.A., Barbosa, E.S.R., Junqueira-Brod, T.C., Gaspar, J.C., Diniz-Pinto, H.S., Sgarbi, P.B.A., and Petrinovic, I.A., 2005, The Late-Cretaceous Goiás alkaline province (GAP), Central Brazil *in* Comin-Chiaramonti, P,, and de Barros Gomes, C., eds., Mesozoic to Cenozoic alkaline magmatism in the Brazilian platform: San Paolo, Edusp/Fapesp, p. 261–316.

Burns, R.G., 1976, The uptake of cobalt into ferromanganese nodules, soils, and synthetic manganese (IV) oxides: Geochimica et Cosmochimica Acta, v. 40, p. 95–102.

Butt, C.R.M., and Cluzel, D., 2013, Nickel laterite ore deposits: Weathered serpentinites: Elements, v. 9, p. 123–128.

Butt, C.R.M., and Nickel, E.H., 1981, Mineralogy and geochemistry of the weathering of the disseminated nickel sulfide deposit at Mt. Keith, Western Australia: Economic Geology, v. 76, no. 6, p. 1736–1751.

Chakhmouradian, A.R., and Mitchell, R.H., 2000, Occurrence, alteration patterns and compositional variation of perovskite in kimberlites: The Canadian Mineralogist, v. 38, p. 975–994.

Cluzel, D., and Vigier, B., 2008, Syntectonic mobility of supergene nickel ores from New Caledonia (southwest Pacific). Evidences from faulted regolith and garnierite veins: Resource Geology, v. 58, p. 161–170.

Colás, V., Padrón-Navarta, J.A., González-Jiménez, J.M., Fanlo, I., Sánchez-Vizcaíno, V.L., Gervilla, F., and Castroviejo, R., 2017, The role of silica in the hydrous metamorphism of chromite: Ore Geology Reviews, v. 90, p. 274–286.

Colin, F., Nahon, D., Trescases, J.J., and Melfi, A.J., 1990, Lateritic weathering of pyroxenites at Niquelandia, Goias, Brazil; the supergene behavior of nickel: Economic Geology, v. 85, p. 1010–1023.

Crundwell, F., Moats, M., Ramachandran, V., Robinson, T., and Davenport, W.G., 2011, Extractive metallurgy of nickel, cobalt and platinum group metals: Oxford, Elsevier, 622 p.

Cui, H., You, L., Feng, X., Tan, W., Qiu, G., and Liu, F., 2009, Factors governing the formation of lithiophorite at atmospheric pressure: Clays and Clay Minerals, v. 57, p. 353–360.

Dalvi, A.D., Bacon, W.G., and Osborne, R.C., 2004, The past and the future of nickel laterites: Prospectors and Developers Association of Canada (PDAC)

2004 International Convention Trade Show and Investors Exchange, Toronto, 2004, Proceedings, p. 1–27.

de Oliveira, S.B., Trescases, J.J., and Melfi, A.J., 1992, Lateritic nickel deposits of Brazil: Mineralium Deposita, v. 27, p. 137–146.

Dowding, C.E., and Fey, M.V., 2007, Morphological, chemical and mineralogical properties of some manganese-rich oxisols derived from dolomite in Mpumalanga province, South Africa: Geoderma, v. 141, p. 23–33.

Dreisinger, D., Golightly, J.P., and Srivastava, R.M., 2008, 43-101 F1 technical report on the Santa Fé and Ipora nickel laterite properties in Brazil for International Nickel Ventures Corporation: InvMetals, www.sedar.com, filed March 11, 2008.

Dublet, G., Juillot, F., Morin, G., Fritsch, E., Fandeur, D., and Brown, G.E. Jr., 2015, Vertical evolution of the crystal-chemistry and crystallinity of goethite upon lateritization of peridotites in New Caledonia: Implications for Ni depletion in lateritic ores: Geochimica et Cosmochimica Acta, v. 160, p. 1–15.

Dublet, G., Juillot, F., Brest, J., Noël, V., Fritsch, E., Proux, O., Olivi, L., Ploquin, F., and Morin, G., 2017, Vertical changes of the Co and Mn speciation along a lateritic regolith developed on peridotites (New Caledonia): Geochimica et Cosmochimica Acta, v. 217, p. 1–15.

Economou-Eliopoulos, M., 2003, Apatite and Mn, Zn, Co-enriched chromite in Ni-laterites of northern Greece and their genetic significance: Journal of Geochemical Exploration, v. 80, p. 41–54.

Elias, M., 2006, Lateritic nickel mineralization of the Yilgarn craton: Society of Economic Geologists, Special Publication 13, p. 1775–1783.

Evans, B.W., and Frost, B.R., 1976, Chrome-spinel in progressive metamorphism—a preliminary analysis, in Irvine, T.N., ed., Chromium: Its physicochemical behavior and petrologic significance: Oxford, Pergamon Press, p. 959–972.

Evans, B.W., Hattori, K., and Baronnet, A., 2013, Serpentinite: What, why, where?: Elements, v. 9, p. 99–106.

Freyssinet, P., Butt, C.R.M., and Morris, R.C., 2005, Ore-forming processes related to lateritic weathering: Economic Geology 100th Anniversary Volume, p. 681–722.

Gibson, S.A., Thompson, R.N., Leonardos, O.H., Dickin, A.P., and Mitchell, J.G., 1995, The Late Cretaceous impact of the Trindade mantle plume: Evidence from large-volume, mafic, potassic magmatism in SE Brazil: Journal of Petrology, v. 36, p. 189–229.

Giovanardi, T., Girardi, V.A., Correia, C.T., Tassinari, C.C., Sato, K., Cipriani, A., and Mazzucchelli, M., 2017, New U-Pb SHRIMP-II zircon intrusion ages of the Cana Brava and Barro Alto layered complexes, Central Brazil: Constraints on the genesis and evolution of the Tonian Goias stratiform complex: Lithos, v. 282, p. 339–357.

Gleeson, S.A., Butt, C.R.M., and Elias, M., 2003, Nickel laterites: A review: SEG Newsletter, no. 54, p. 1, 12–18.

Golightly, J.P., 2010, Progress in understanding the evolution of nickel laterites: Society of Economic Geologists, Special Publication 15, p. 451–475.

González-Jiménez, J.M., Kerestedjian, T., Proenza Fernández, J.A., and Gervilla Linares, F., 2009, Metamorphism on chromite ores from the Dobromirtsi ultramafic massif, Rhodope mountains (SE Bulgaria): Geologica Acta, v. 7, p. 413–429.

Herrington, R., Mondillo, N., Boni, M., Thorne, R., and Tavlan, M., 2016, Bauxite and nickel cobalt lateritic deposits of the Tethyan belt: Society of Economic Geologists, Special Publication 19, p. 349–387.

Horn, I., Foley, S.F., Jackson, S.E., and Jenner, G.A., 1994, Experimentally determined partitioning of high field strength and selected transition elements between spinel and basaltic melt: Chemical Geology, v. 117, p. 193–218.

Kay, J.T., Conklin, M.H., Fuller, C.C., and O'Day, P.A., 2001, Processes of nickel and cobalt uptake by a manganese oxide forming sediment in Pinal Creek, Globe mining district, Arizona: Environmental Science and Technology, v. 35, p. 4719–4725.

Lacerda Filho, J.V., Rezende, A., and Silva, A., 2000, Geologia e Recursos Minerais do Estado de Goiás e Distrito Federal (SIG-Goiás): Programa Levantamento Geológico Básico (PLGB), scale 1:500,000, Companhia Brasileira de Recursos Minerais/Metais de Goiás (CPRM/METAGO)/Universidade de Brasília, 184 p.

Lambiv Dzemua, G., and Gleeson, S.A., 2012, Petrography, mineralogy, and geochemistry of the Nkamouna serpentinite: Implications for the formation of the cobalt-manganese laterite deposit, southeast Cameroon: Economic Geology, v. 107, p. 25–41.

Lambiv Dzemua, L., Gleeson, S.A., and Schofield, P.F., 2013, Mineralogical characterization of the Nkamouna Co-Mn laterite ore, southeast Cameroon: Mineralium Deposita, v. 48, p. 155–171.

Manceau, A., Charlet, L., Boisset, M.C., Didier, B., and Spadini, L., 1992, Sorption and speciation of heavy metals on hydrous Fe and Mn oxides. From microscopic to macroscopic: Applied Clay Sciences, v. 7, p. 201–223.

Martín-Fernández, J.A., Barceló-Vidal, C., and Pawlowsky-Glahn, V., 2003, Dealing with zeros and missing values in compositional data sets using nonparametric imputation: Mathematical Geology, v. 35, p. 253–278.

McKenzie, R.M., 1989, Manganese oxides and hydroxides, in Dixon, J.B., Weed, S.B., and Dinauer, R.C., eds., Minerals in soil environments, 2nd ed.: Madison, Wisconsin, Soil Science Society of America, p. 439–465.

Melfi, A.J., Trescases, J.J., and Barros de Oliveira, S.M., 1979, Les "laterites" nickeliferes du Brésil: Cahiers ORSTOM. Série Géologie, v. 11, p. 15–42.

Mellini, M., Rumori, C., and Viti, C., 2005, Hydrothermal reset of magmatic spinels in retrograde serpentinites: Formation of "ferritchromit" rims and chlorite aureoles: Contributions to Mineralogy and Petrology, v. 149, p. 266–275.

Merlini, A., Grieco, G., and Diella, V., 2009, Ferritchromite and chromianchlorite formation in mélange-hosted Kalkan chromitite (southern Urals, Russia): American Mineralogist, v. 94, p. 1459–1467.

Mével, C., 2003, Serpentinization of abyssal peridotites at mid-ocean ridges: Comptes Rendus: Geoscience, v. 335, p. 825–852.

Mudd, G.M., and Jowitt, S.M., 2014, A detailed assessment of global nickel resource trends and endowments: Economic Geology, v. 109, p. 1813–1841.

Mysen, B., 2007, Partitioning of calcium, magnesium, and transition metals between olivine and melt governed by the structure of the silicate melt at ambient pressure: American Mineralogist, v. 92, p. 844–862.

Noack, Y., and Colin, F., 1986, Chlorites and chloritic mixed-layer minerals in profiles on ultrabasic rocks from Moyango (Ivory Coast) and Angiquinho (Brazil): Clay Minerals, v. 21, p. 171–182.

Ożóg, M., and Pieczonka, J., 2019, Chemistry of primary and altered Cr-spinels in chromitites and peridotites from the ophiolitic massif in SE Kosovo: Society for Geology Applied to Mineral Deposits (SGA), Biennial Meeting, 15th, Glasgow, Scotland, August 27–39, 2019, Proceedings, v. 2, p. 573–576.

Pimentel, M.M., Fuck, R.A., Jost, H., Ferreira-Filho, C.F., and Araujo, S.M., 2000, The basement of the Brasilia fold belt and the Goiás magmatic arc, in Cordani, U.G., Milani, E.J., Thomaz-Filho, A., and Campos, D.A., eds., Tectonic evolution of South America: Geological Society of America, p. 195–229.

Pimentel, M.M., Ferreira Filho, C.F., and Amstrong, R.A., 2004, Shrimp U-Pb and Sm-Nd ages of the Niquelandia layered complex: Meso (1.25 Ga) and Neoproterozoic (0.79 Ga) extensional events in Central Brasil: Precambrian Research, v. 132, p. 132–135.

Pimentel, M.M., Ferreira Filho, C.F., and Armele, A., 2006, Neoproterozoic age of the Niquelândia Complex, Central Brazil: Further ID-TIMS and Sm-Nd isotopic evidence: Journal of South American Earth Sciences, v. 21, p. 228–238.

Porto, C.G., 2016, Geochemical exploration challenges in the regolith dominated Igarapé Bahia gold deposit, Carajás, Brazil: Ore Geology Reviews, v. 73, p. 432–450.

Putzolu, F., Balassone, G., Boni, M., Maczurad, M., Mondillo, N., Najorka, J., and Pirajno, F., 2018, Mineralogical association and Ni-Co deportment in the Wingellina oxide-type laterite deposit (Western Australia): Ore Geology Reviews, v. 97, p. 21–34.

Putzolu, F., Boni, M., Mondillo, N., Maczurad, M., and Pirajno, F., 2019, Ni-Co enrichment and high-tech metals geochemistry in the Wingellina Ni-Co oxide-type laterite deposit (Western Australia): Journal of Geochemical Exploration, v. 196, p. 282–296.

Ratié, G., Jouvin, D., Garnier, J., Rouxel, O., Miska, S., Guimarães, E., Viera, C., Sivry, Y., Zelano, I., Montarges-Pelletier, E., Thil, F., and Quantin, C., 2015, Nickel isotope fractionation during tropical weathering of ultramafic rocks: Chemical Geology, v. 402, p. 68–76.

Ratié, G., Quantin, C., Jouvin, D., Calmels, D., Ettler, V., Sivry, Y., Viera, C., Ponzevera, E., and Garnier, J., 2016, Nickel isotope fractionation during laterite Ni ore smelting and refining: Implications for tracing the sources of Ni in smelter-affected soils: Applied Geochemistry, v. 64, p. 136–145.

Reimann, C., Filzmoser, P., and Garrett, R.G., 2002, Factor analysis applied to regional geochemical data: Problems and possibilities: Applied Geochemistry, v. 17, p. 185–206.

Reimann, C., Filzmoser, P., Garrett, R., and Dutter, R., 2011, Statistical data analysis explained: Applied environmental statistics with R: Chichester, United Kingdom, Wiley, 343 p.

Roqué-Rosell, J., Mosselmans, F., Proenza, J.A., Labrador, M., Galí, S., Atkinson, K.D., and Quinn, P.D., 2010, Sorption of Ni by "lithiophorite-asbolane"

intermediates in Moa Bay lateritic deposits, eastern Cuba: Chemical Geology, v. 275, p. 9–18.

Sonoki, I.K., and Garda, G.M., 1988, K-Ar ages of alkaline rock from southern Brazil and eastern Paraguay: Compilation and adaptation of new decay constants: Boletim IG-USP, v. 19, p. 63–85.

Suárez, S., Nieto, F., Velasco, F., and Martín, F.J., 2011, Serpentine and chlorite as effective Ni-Cu sinks during weathering of the Aguablanca sulphide deposit (SW Spain). TEM evidence for metal-retention mechanisms in sheet silicates: European Journal of Mineralogy, v. 23, p. 179–196.

Tan, W., Liu, P., He, H., Wang, C.Y., and Liang, X., 2016, Mineralogy and origin of exsolution in Ti-rich magnetite from different magmatic Fe-Ti oxidebearing intrusions: The Canadian Mineralogist, v. 54, p. 539–553.

Tauler, E., Lewis, J.F., Villanova-de-Benavent, C., Aiglsperger, T., Proenza, J.A., Domènech, C., Gallardo, T., Longo, F., and Galí, S., 2017, Discovery of Ni-smectite-rich saprolite at Loma Ortega, Falcondo mining district (Dominican Republic): Geochemistry and mineralogy of an unusual case of "hybrid hydrous Mg silicate-clay silicate" type Ni-laterite: Mineralium Deposita, v. 52, p. 1011–1030.

Taylor, R.M., McKenzie, R.M., and Norrish, K., 1964, The mineralogy and chemistry of manganese in some Australian soils: Soil Research, v. 2, p. 235–248.

Teitler, Y., Cathelineau, M., Ulrich, M., Ambrosi, J.P., Munoz, M., and Sevin, B., 2019, Petrology and geochemistry of scandium in New Caledonian Ni-Co laterites: Journal of Geochemical Exploration, v. 196, p. 131–155.

Thorne, R., Herrington, R., and Roberts, S., 2009, Composition and origin of the Çaldağ oxide nickel laterite, W. Turkey: Mineralium Deposita, v. 44, p. 581–595.

Toffolo, L., Nimis, P., Tret'yakov, G.A., Melekestseva, I.Y., and Beltenev, V.E., 2020, Seafloor massive sulfides from mid-ocean ridges: Exploring the causes of their geochemical variability with multivariate analysis: Earth-Science Reviews, v. 201, article 102958.

U.S. Geological Survey, 2020, Mineral commodity summaries 2020: U.S. Geological Survey, 200 p., doi: 10.3133/mcs2020.

Valeriano, C.D.M., Pimentel, M.M., Heilbron, M., Almeida, J.C.H., and Trouw, R.A.J., 2008, Tectonic evolution of the Brasília belt, Central Brazil, and early assembly of Gondwana: Geological Society of London, Special Publication 294, p. 197–210.

Valix, M., and Cheung, W.H., 2002, Study of phase transformation of laterite ores at high temperature: Minerals Engineering, v. 15, p. 607–612.

Van Decar, J.C., James, D.E., and Assumpção, M., 1995, Seismic evidence for a fossil mantle plume beneath South America and implications for plate driving forces: Nature, v. 378, p. 25–31.

Velde, B.B., and Meunier, A., 2008, The origin of clay minerals in soils and weathered rocks: Amsterdam, Springer Science and Business Media, 418 p.

Villanova-de-Benavent, C., Proenza, J.A., Galí, S., García-Casco, A., Tauler, E., Lewis, J.F., and Longo, F., 2014, Garnierites and garnierites: Textures, mineralogy and geochemistry of garnierites in the Falcondo Ni-laterite deposit, Dominican Republic: Ore Geology Reviews, v. 58, p. 91–109.

Villemant, B., Jaffrezic, H., Joron, J.L., and Treuil, M., 1981, Distribution coefficients of major and trace-elements - fractional crystallization in the alkali basalt series of Chaine-Des-Puys (Massif Central, France): Geochimica et Cosmochimica Acta, v. 45, p. 1997–2016.

Wiewióra, A., and Szpila, K., 1975, Nickel containing regularly interstratified chlorite-saponite from Szklary, Lower Silesia, Poland: Clays and Clay Minerals, v. 23, p. 91–96.

Francesco Putzolu is a Ph.D. candidate in economic geology at the Department of Earth Sciences, Environment and Resources of the University of Naples Federico II (Italy), where he also received M.Sc. and B.Sc. degrees. His current research concerns the mineralogical and geochemical footprint, as well as the genetic processes, of Ni-Co laterite, bauxite, and clay-bearing Zn nonsulfide ores.